Recent Progress on Interface Engineering for High-Performance, Stable Perovskites Solar Cells

Yiyi Zhu, Swapnadeep Poddar, Lei Shu, Yu Fu, and Zhiyong Fan*

Rapid progress in the domain of perovskite solar cells (PSCs) has boosted the power conversion efficiency (PCE) of such cells to 25.2%. However, the long-term stability of a high-performance PSCs is still the foremost concern that hinders its practical application. The interfaces are considered as the key part that determines the overall device performance and longevity. These interfaces include the intralayer grain boundaries (GBs) inside the perovskites, the interface between perovskites with electron/hole transport layer (ETL/HTL), and the interface of ETL/HTL with top/down contacts. To acquire a deep and detailed understanding of the impacts of interfacial properties, herein, a concise overview of recent interfacial engineering strategies with the aim of minimizing traps, promoting carrier extraction, and improving stability are summarized.

1. Introduction

Solar energy is the most abundant and ecofriendly source of renewable energy. The newly emerged organic–inorganic halide perovskite (PVSK) materials with the structure of ABX_3 wherein A is methylammonium (MA), formamidinium (FA), or cesium (Cs); B is Pb or Sn; and X is Cl, Br, or I, are promising candidates for photovoltaic systems. Over the past seven years, the power conversion efficiency (PCE) of perovskite solar cells (PSCs) has increased at an unprecedented rate, with efficiency currently touching 25.2% (certified) in 2019.[1,2] The exponential progress can be attributed to the excellent photo-electronic properties of PVSK, including high carrier lifetime, long diffusion length, high light absorbance, etc., and its low-temperature processability reduces the energy cost associated with manufacturing.

High-performance PSCs are dominated by 3D PVSK, for instance, $MAPbI_3$, $FAPbI_3$, and their mixtures. Regardless of the promising properties of PVSK, the high-performance device relies on the efficient extraction of the photogenerated carriers before their recombination. The charge extraction efficiency plays a pivotal role in the photovoltaic performance in terms of current density (J_{sc}) and fill factor (FF). Notably, the photoinduced charge separation and collection junction is the boundary between PVSK with electron/hole transport layer (ETL/HTL) at which photogenerated excitons are dissociated into charge carriers. Therefore, appropriate interfacial band bendings, a better interface quality are effective strategies toward developing highly efficient cells. In addition, the poor contacts at the interfaces between various layers result in a low charge extraction efficiency and high series resistance.[3] Besides, the nonradiative recombination caused by the defects and impurities at PVSK grain boundaries (GBs) are the leading causes for the open-circuit voltage (V_{oc}) loss.[4–8]

The long-term stability of PSCs and their degradation mechanism is under intense investigation.[9] Researchers have witnessed the rapid degradation of 3D PVSK when it is exposed to moisture, oxygen, elevated temperature, and UV light.[10] The primary reason for the instability is the moisture-induced degradation.[11] Apart from the inherent stability of PVSK, the stability issue of PSCs is also related to other constituent material and interfacial properties in the cells. Recent studies have already demonstrated that GBs provide an infiltrating pathway for oxygen and moisture and subsequently cause the decomposition of the entire film.[12] By forming highly ionic-conducting pathways, GBs aggravate hysteresis during device operation.[13–16] And hysteresis behavior interferes with PVSK degradation processes. Consequently, interface engineering for efficient and stable PSCs is a realistic path toward a commercially viable device.

In this review, we discussed the influence of interfacial charge recombination, extraction, collection on the performance of PSCs, as well as the degradation process and hysteresis behavior of perovskite systems. Furthermore, we summarized the impacts of defects at GBs for a better understanding of the role of GBs. In particular, we focus on interface engineering pertaining to the performance and longevity of PSCs. We have surveyed recent interface engineering developments toward stable, high-performance PSCs, which includes strategies for the large-crystal PVSK thin films, passivation of GBs, multidimensional PVSK, and better energy-band alignment in a cell. Finally, we reviewed prospects in the field.

Y. Zhu, S. Poddar, L. Shu, Y. Fu, Prof. Z. Fan
HKUST-Shenzhen Research Institute
No. 9 Yuexing first RD, South Area, Hi-tech Park, Nanshan
Shenzhen 518057, China
E-mail: eezfan@ust.hk
Y. Zhu, S. Poddar, L. Shu, Y. Fu, Prof. Z. Fan
Department of Electronic and Computer Engineering
Hong Kong University of Science and Technology (HKUST)
Clear Water Bay, Kowloon, Hong Kong SAR, China

The ORCID identification number(s) for the author(s) of this article can be found under https://doi.org/10.1002/admi.202000118.

2. The Impacts of GBs

Defects at GBs in the polycrystalline thin films are unavoidable, and they play a critical role in optoelectronic properties as previously reported for GaAs,[17–19] CdTe,[20,21] poly-Si,[22] and copper indium gallium selenide (CIGS).[21,23] This is due to the significantly changed charge carrier dynamics by the vacancies, interstitials, distorted bond angles and bond distances at the GBs.[24] Different from the materials mentioned above, PVSK was reported to be a promising photovoltaic candidate with a high defect tolerance.
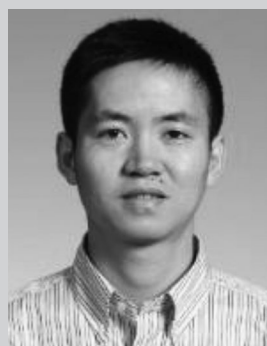
Density-functional studies show that intrinsic bulk defects (i.e., Schottky defects and Frenkel defects) do not create deep trap states.[25] The illustration of ideal crystal, Schottky defects, and Frenkel defects can be found in **Figure 1**a–c. The Schottky defects, for instance, PbI_2 and MAI vacancy, do not create a trap state. However, they diminish carrier lifetime. Frenkel defects, for instance, Pb, I, and MA vacancies form shallow levels near band edges.[25] The first principle density-functional theory calculations were performed by Yin et al.[26] The result shows that dominant point defects inside $MAPbI_3$ grain are interior form shallow states. However, shown in Figure 1f, the antisites donate deep-level trap states in PVSK.[27] This illustrates that the Pb—Pb and I—I wrong bonds form deep-level trap states. To understand the interaction of two grain at GBs, models of polycrystal $MAPbI_3$ with different distances between two GBs were constructed.[28] The result shows that when the widths between two GBs reach 38.32 Å, there will be no I—I wrong bond and Pb—Pb wrong bond at GBs. Such a distance will make the interaction of two grain negligible. The defects at GBs mainly contain dangling bonds. The benign GBs properties could be attributed to the shallow defects states made by the dangling bonds. On the other hand, a study illustrated that the I—I wrong bond at PVSK GBs (Figure 1d) only creates shallow states close to the valance band maximum(VBM).[29] These results explain why polycrystalline PVSK has excellent charge transporting property and high V_{oc} compared with other photovoltaic thin films. The shallow defects states are not as crucial as the deep-level trap states. However, a study shows that the shallow defects created by I—I wrong bond at GBs trap holes and increases the effective mass of holes.[29]

Even though simulations show that the intrinsic defects in PVSK are benign, experimental observations prove that defects at GBs accelerate the nonradiative recombination and deteriorate PVSK optoelectronic properties in terms of carrier diffusion length,[30,31] carrier lifetime,[32,33] mobility,[34] etc. Carrier lifetime and diffusion length are commonly used as indicators of PVSK quality. The measured diffusion length of the $MAPbI_3$ single crystal is 175 mm under 1 sun (100 mW cm^{-2}) illumination.[30] Whereas, the diffusion length of polycrystalline $MAPbI_3$ film is in the order of 100 nm.[35] The photoluminescence (PL) time decay trace on a $MAPbI_3$ single crystal was performed. The carrier lifetime for $MAPbI_3$ single crystal was estimated to be $\tau \approx 22$ and 1032 ns with biexponential fits.[32] The huge carrier lifetime and diffusion length suggest that photogenerated carriers encounter GBs before recombination.[36] Moreover, $MAPbI_3$ GBs are explicitly associated with PL quenching, which was verified in confocal fluorescence microscopy correlated with scanning electron microscopy.[31] This result also

Yiyi Zhu received her bachelor's and master' degrees in Materials Science and Engineering from Central South University, China. She is currently a Ph.D. student in the Department of Electrical Engineering and Computer Sciences at Hong Kong University of Science and Technology under the supervision of Prof. Zhiyong Fan. Her research focuses on developing highly efficient and stable perovskite photovoltaics.

Zhiyong Fan received his B.S. and M.S. degrees in physical electronics from Fudan University, Ph.D. degree from University of California, Irvine in Materials Science. From 2007 to 2010, he worked in University of California, Berkeley as a postdoctoral fellow in department of Electrical Engineering and Computer Sciences, with a joint appointment with Lawrence Berkeley National Laboratory. In May 2010, he joined the faculty of Hong Kong University of Science and Technology and currently he is a professor at Department of Electronic and Computer Engineering. His interests are on the design and fabrication of novel nanostructures and nanomaterials for high-performance optoelectronics, energy harvesting devices, and sensors.

suggests that GBs are not as benign as previous theoretical calculations.[26]

These raise the question as to why GBs accelerate the electron–hole recombination. Long et al.[36] witnessed notably accelerated nonradiative recombination at $MAPbI_3$ GBs by using non-adiabatic molecular dynamics combined with time-domain density functional theory. Their work revealed that the defects at GBs reduce the bandgap and enhance the electron–phonon non-adiabatic coupling. Similarly, Duan et al.[37] identified defect state distribution in the $MAPbI_3$ and revealed a defect state ≈ 0.16 eV above the VBM through admittance spectroscopy. Based on their theoretical calculations, the defect state is probably due to iodide interstitials serving as nonradiative recombination centers. Bischak et al.[38] observed significant GBs accelerated electron–hole recombination in polycrystalline $MAPbI_3$ thin film through cathodoluminescence microscopy.

The hysteresis behavior is another hindrance for PVSK materials to achieve reliable high performance. The possible mechanisms for hysteresis were trapping and detrapping of carriers, ferroelectric property, and ion migration. GBs are proved to be
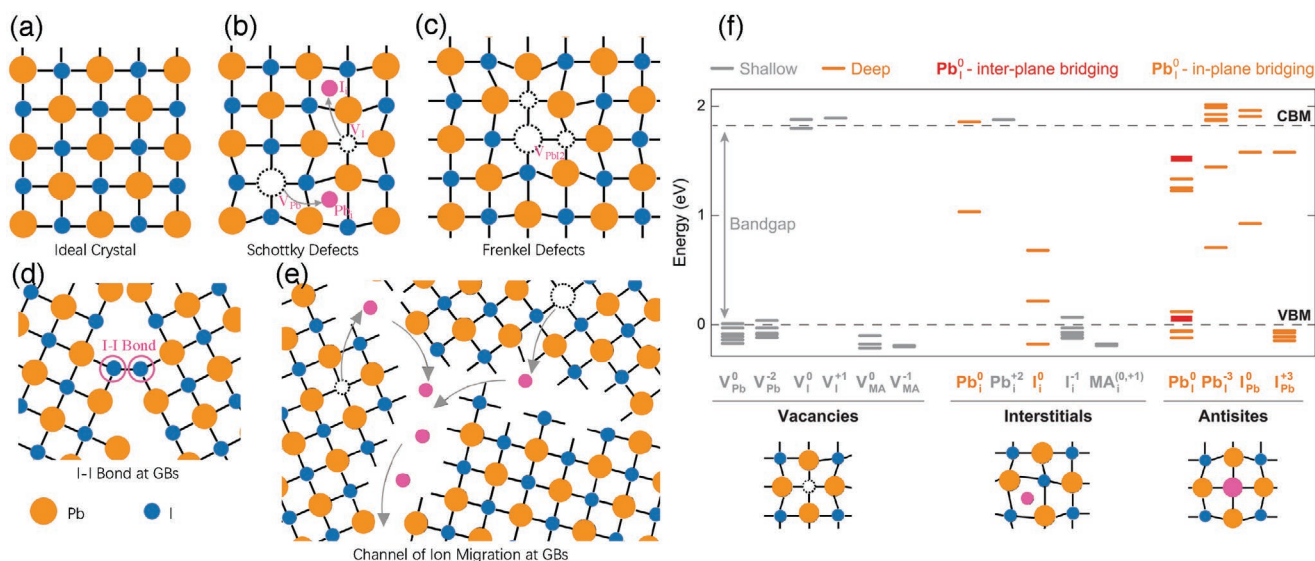
**ADVANCED
SCIENCE NEWS**

www.advancedsciencenews.com

**ADVANCED
MATERIALS
INTERFACES**

www.advmatinterfaces.de

Figure 1. Illustration of a) ideal crystal, b) Schottky defects of vacancies (V_{Pb}, V_{I},) and interstitials (Pb$_i$, I$_i$), c) Frenkel defects of vacancies (V_{PbI2}), d) I—I Bond at GBs. e) The channel of ion migration facilitated by open space and dangling bonds at GBs. f) Energy levels associated with the defect states corresponding to neutral and charged vacancies (V_{Pb}, V_{I}, V_{MA}), neutral and charged interstitials (Pb$_i$, I$_i$, MA$_i$), and neutral and charged states associated with antisites (Pb$_I$ and I$_{Pb}$). f) (Upper part) Reproduced with permission.[27] Copyright 2015, American Chemical Society.

charge accumulation sites and accelerate hysteresis behavior. Furthermore, compared with vacancy assisted ion migration inside the grain interior, the ion migration activation energy at GBs is much lower.[15] This can be ascribed to the more open space, dangling bonds and lattice distortion at GBs.[16] Figure 1e illustrated the channel of ion migration facilitated by open space and dangling bonds at GBs. Therefore, GBs are short-cuts for ion migration and aggravate the undesired hysteresis behavior of PVSK solar cells. Moreover, GBs provide the penetration pathway for oxygen and moisture, thereby GBs consider as the most vulnerable sites for PVSK degradation.[12,39,40]

3. Intralayer Engineering

3.1. Large Crystal Engineering

To address unfavorable issues associated with GBs, minimizing the PVSK intralayer GBs area is a practical approach.[41] In this section, we have reviewed the approaches toward large crystal PVSK thin film, for instance, the solvent-annealing,[42–46] hot-casting method,[34] successive drop method,[47] introducing additives,[48] etc.

Solvent-annealing, where solvent vapor induced during annealing, is a feasible way to slow down the crystallization process and achieve high-quality PVSK thin film. Wang et al.[42] obtained high crystallinity MAPbI$_3$ films with grain size over 5 mm through a solvent annealing method. Verified in the PL characterization and impedance spectroscopy analysis results (**Figure 2**a–d), the defects states of PVSK thin film via pyridine-annealing were significantly reduced. Benefiting from the superior crystallinity, the device based on solvent-annealing delivered a PCE of 14.13%, which is a 50% enhancement in efficiency compared with conventional thermally annealed one. Similarly, Xiao et al.[43] achieved high crystallinity MAPbI$_3$ film

with grain size over 1 μm under the annealing atmosphere of N,N-dimethylformamide (DMF) vapor. The density of trap states (Figure 2e) in MAPbI$_3$ thin films from solvent-annealed was significantly reduced in comparison with the thermal-annealed one, which was confirmed in thermal admittance spectroscopy measurement.

Moreover, based on the transient photovoltage and photocurrent results shown in Figure 2f,g, the carrier lifetime and transit mobility were remarkably improved after solvent-annealing. The impact of solvent-annealing conditions on the MAPbI$_3$ thin film was studied by Liu et al.[44] They have investigated different atmospheric conditions, including N$_2$, H$_2$O, γ-butyrolactone (GBL), DMF, and dimethyl sulfoxide (DMSO). After the optimization of annealing condition, the crystallinity of PVSK was significantly improved. The defect density of PVSK is reduced due to the improved crystallinity. Furthermore, the contacts at the interface between PVSK and ETL/HTL were remarkably improved, which is critical for efficient charge separation and collection. With improved crystallinity and better contacts, the DMSO-treated films delivered a PCE of over 13%. Giesbrecht et al.[45] obtained large crystal MAPbBr$_3$ thin film (grain size 5–10 μm) with highly ordered orientation via a vapor-assisted solution process. The highly ordered PVSK grains, in combination with high crystallinity, significantly enhanced the charge collection efficiency. As a result, an internal quantum efficiency exceeding 95% was obtained. Tosun and Hillhose[46] achieved large crystal MAPbI$_{3−x}$Cl$_x$ thin films by annealing PVSK thin film in the presence of MAI vapor. Moreover, they observed enhanced lifetimes with the raise of grain size.

Apart from the solvent-annealing method, recent studies demonstrated that continuous and homogeneous PVSK thin film can be achieved by balancing the competition between the solvent evaporation rate, solute diffusion rate, and perovskite growth rate and etc.[49] The polymer [poly(methyl methacrylate),
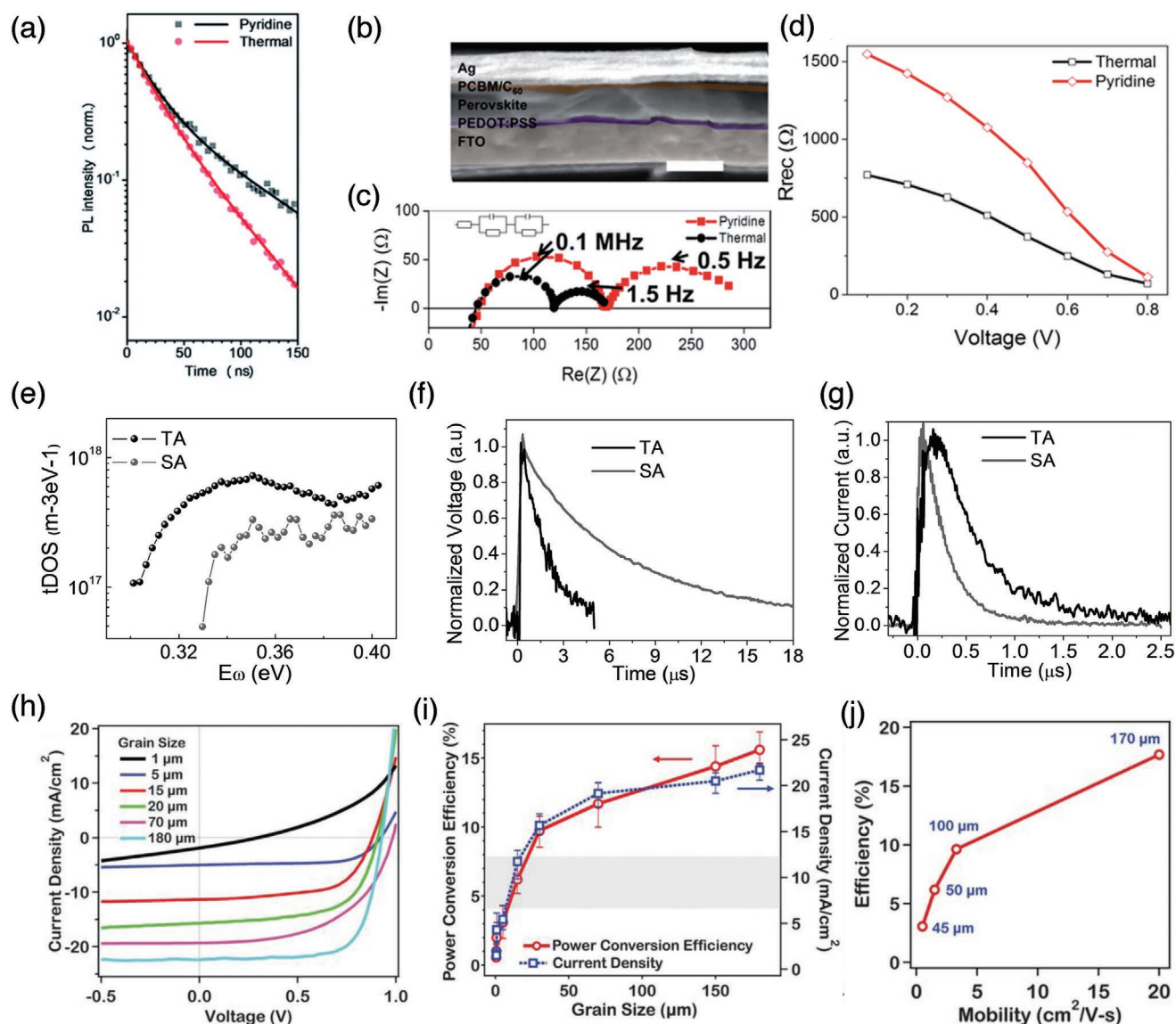
ADVANCED
SCIENCE NEWS
www.advancedsciencenews.com

ADVANCED
MATERIALS
INTERFACES
www.advmatinterfaces.de

Figure 2. a) The transient photoluminescence decay kinetics of the solvent-annealed (black) and thermally annealed (red) PVSK films. b) Cross-sectional SEM images of solvent annealed device (the scale bar is 500 nm). c) Nyquist plot of the impedance spectroscopy of the devices biased at 0.8 V under illumination. d) The fitted recombination resistance at different bias voltages of the solar cells, based on the inserted equivalent circuit in (c). a–d) Reproduced with permission.[42] Copyright 2016, Royal Society of Chemistry. e) Trap density of states for the solvent-annealed device (SA) and thermal-annealed device (TA) calculated from the thermal admittance spectroscopy measurement. f) Photovoltage decay under 0.3 sun illumination measured by transient photovoltage techniques. g) Photocurrent decay measured by transient photocurrent techniques. e–g) Reproduced with permission.[43] Copyright 2014, Wiley-VCH. h) Current-density–voltage (J–V) curves obtained under AM 1.5 illumination. i) Average overall PCE (left) and J_{sc} (right) as a function of crystalline grain size. The average values were obtained by averaging the PCE and J_{sc} for 25 devices; error bars were calculated by subtracting the average value from max or min values. Gray box represents the range of PCE values obtained using the conventional post-annealing process. j) The PCE values appear to be correlated to the bulk mobility of the absorber (labels correspond to the average grain size). h–j) Reproduced with permission.[34] Copyright 2015, American Association for the Advancement of Science.

(PMMA)][50] is found to be an additive that can decrease the PVSK nucleation free energy barrier[51] and facilities the heterogeneous nucleation. Moreover, after the introduction of PMMA, the growth rate of PVSK was slowed down by forming an intermediate adduct.[52] As a result, larger oriented PVSK grains with a lower density of traps states were fabricated, which enable PSCs with a PCE over 21% was achieved. Through a solution-based hot-casting method, Nie et al.[34] obtained MAPbI$_{3−x}$Cl$_x$

thin films with grain size over millimeters. A strong correlation between the PVSK thin film morphology and device performance was identified in their work. Figure 2h,i demonstrated the J–V curves of PSCs based on different grain size PVSK obtained under air mass (AM) 1.5 illumination. The PCE has been remarkably enhanced with the increase of grain size. The V_{oc} was enhanced from 0.4 to 0.94 V and FF from 0.4 to 0.83. Besides, the unfavorable hysteresis during device operation

**ADVANCED
SCIENCE NEWS**
www.advancedsciencenews.com

**ADVANCED
MATERIALS
INTERFACES**
www.advmatinterfaces.de

was remarkably suppressed. Shown in Figure 2j, higher carrier mobility was achieved in the PVSK thin film with larger grains size. The improved mobility can be ascribed to reduced trap density of states in large crystal PVSK thin film allowing for the photogenerated electron/hole to move in the cell without constantly encounters with traps. Dong et al.[47] proposed a successive drop method to modulate the $MAPbI_{3x}Cl_x$ grain growth and achieved a well-oriented $MAPbI_{3x}Cl_x$ thin film with a grain size up to 3 µm. Liang et al.[48] proposed a practical approach to facilitate homogenous nucleation of $MAPbI_{3x}Cl_x$ by introducing additives into the precursor solution. The processing additives facilitate nucleation and modify the growth kinetics simultaneously. Li et al.[41] proposed a novel colloidal strategy to fabricate monolayer PVSK thin films with a grain size up to 3 µm. Their work showed that the grain size of PVSK was controlled by controlling the size of colloidal clusters. Moreover, the colloidal clusters can be well organized on the substrate by spin-coating the precursor solution incorporated with mixed MACl and DMS. Owning to the high-quality of PVSK thin film, a PCE of 19.14% was obtained in their work. Tavakoli et al.[53] developed a novel solvent-free process to fabricate less-toxic $MA(Sn_xPb_{1-x})I_3$ film and achieved a PCE of 14.04%. By using Pb–Sn eutectic alloy, $MA(Sn_xPb_{1-x})I_3$ thin film with grain sizes up to 5 µm were synthesized directly from liquid phase metal. Benefiting from high crystallinity, a record PCE of 14.04% for Sn-rich PVSK was achieved. Kam et al.[54] reported an all-vacuum sequential deposition method to fabricate $MA_yFA_{1-y}PbI_xBr_{3-x}$ based PSCs. A uniform and compacted PVSK thin film with a grain size of 3.5 µm was acquired in their process. Tavakoli et al.[55] present a vapor deposition technique of highly crystalline PVSK thin films by layer-by-layer deposition of PbI_2 and MAI.

3.2. Grain Surface Passivation

A surplus of charge accumulating at the PVSK crystal surface, stemming from these uncoordinated ions (dangling bonds), accelerates the recombination at GBs[56] and interferes with the degradation process.[2] Especially, the defects at the interface between PVSK and ETL/HTL deteriorate carrier collection and extraction, hinder the further enhancement of device performance. GBs passivation by molecules or polymers has been confirmed as a feasible way to reduce the concentration of traps or defects at GBs. Besides, physical covering PVSK crystal surface with hydrophobic materials can stabilize the PVSK thin film and provide device moisture-tolerance. In this section, we have summarized the present strategies in mitigating the negative effect of GBs.

In general, the poly-crystallinity PVSK thin film has a high percentage of uncoordinated ions at the grain surface.[57,58] The uncoordinated ions capture photogenerated carriers, accelerate nonradiative recombination, and severely reduce the carrier lifetime.[50] This in turn results a loss of V_{oc} and an overall performance of a solar cell. Therefore, the formation of chemical bonds with uncoordinated ions is a common and practical approach to suppress these defects. Lewis acids, phenyl-C61-butyric acid methyl ester (PCBM),[59,60] iodopentafluorobenzene (IPFB)[61] for example, are ideal candidates to passivate the

negative-charged defects (e.g., Pb-I antisite, uncoordinated I⁻) at GBs. This is because Lewis acids, which possess electron-conducting property, can accept electrons from negative-charged defects.

On the other hand, chlorine incorporation in $MAPbI_3$ leads to a lower the electron–hole recombination rate,[31,62,63] enhanced the carrier lifetime,[64,65] and a longer diffusion length.[62] The photon-generated charges in $MAPbI_{3x}Cl_x$ thin film exhibit diffusion length up to 1 µm,[62] which is a tenfold enhancement compared to $MAPbI_3$ thin film.[35] However, there are still controversial opinions toward the mechanism of chlorine incorporation. Tidhar et al.[64] and Williams et al.[65] attributed the improved performance to the better crystal coalescence in the presence of chlorine. The theoretical calculation of Long et al.[36] also suggests that chlorine doping slows down non-radiative recombination and elongates excited-state lifetime. Whereas Long et al.[36] believe that chlorine will replace iodine, and substitutionally present at the grain surface of $MAPbI_3$. The presence of chlorine restores the non-adiabatic coupling close to the value witnessed in pristine $MAPbI_3$.

The electron donor Lewis-base (e.g., thiophene,[2,66] lead (II) oxysalt,[67] and pyridine[2,31,68]) can suppress the positively charged defects at PVSK grain surface (e.g., uncoordinated Pb^{2+}). Reported by Yang et al.,[67] the concentration of defects was decreased by covering the PVSK grain surface with wide-bandgap lead (II) oxysalt. The reduced traps states and elongated carrier lifetime boost the device PCE up to 21.1%. Moreover, the moisture-tolerance of the device was significantly improved after surface modification. Noel et al.[2] utilized the Lewis bases thiophene and pyridine with the intention of surface treatment of $MAPbI_{3x}Cl_x$. They observed remarkably inhibited nonradiative recombination within the treated $MAPbI_{3x}Cl_x$, achieving lifetimes up to 2 µs, which is nearly one order of magnitude enhancement compared with the control group. They ascribed the enhanced lifetime to the passivation of uncoordinated Pb^{2+} within the crystal.

Nevertheless, most of Lewis acid or base approaches can only suppress either positive or negative charged defects. Therefore, it is desirable to taken charged neutrality passivation into consideration. Reported by Zheng et al.[69] different types of positive and negative charged defects in PVSK were effectively passivated by quaternary ammonium halides, which result in an efficient and stable PSCs (PCE = 20.59 ± 0.45%, certified). Similarly, the alkyl phosphonic acid ω-ammonium chlorides were also reported as promising candidates for the chemical passivation of the PVSK grain surface.[70] Interestingly, apart from the passivation of PVSK, alkyl phosphonic acid ω-ammonium chlorides perform as growth-controlling agents simultaneously facilitating the formation of a homogeneous and close-packed PVSK thin film.

Different from passivation strategies used silicon solar cells, which generally involve the formation of chemical bonds with uncoordinated ions, the passivation strategies for PSCs should also consider the undesirable chemical reaction during PVSK formation as well as the moisture-induced degradation of PVSK. The desorption of MA occurs during the thermal annealing of $MAPbI_3$, which causes the formation of vacancies (uncoordinated ions) and Pb-I antisite defects.[71] The desorption of MA forms potential wells at GBs for carriers and leads to severe

trapping, charge accumulation, and recombination.[26,72,73] To diminish the detrimental effect from the loss of MAI during PVSK annealing, a Lewis acid–base adduct approach was proposed by Son et al.[74] By incorporating 6 mol% excess MAI into the precursor solution, an MAI layer was assembled at GBs during the formation of MAPbI$_3$. It is found that the MAI layer improved the hole–electron extraction and reduced the hysteresis behavior of PSCs. In addition, the presence of PbI$_4^-$ species in the DMF solution, or [(Pb$_3$I$_8$)$_n$]$^{2n-}$ in DMSO mediator, may cause the formation of interstitial iodine which are deep-level defects.[75–77] To reduce the concentration of deep-level defects caused by interstitial iodine, Yang et al.[77] tried to introduce additional iodide ions during the PVSK formation. Their process boosts the certified efficiency of PSCs to 19.7% with an active area of 1 cm^2.

Some neutral structural defects, which might not be covered by passivation additives, can aggravate PVSK degradation. For instance, the disordered MAI at GBs will facilitate the permeation of moisture and accelerate the PVSK decomposition.[78] Therefore, it is highly desirable to cover PVSK grain surface with a hygroscopic scaffold (e.g., phenethyl ammonium cation (PEA$^+$),[79,80] n-butylammonium (BA$^+$),[81] poly(ethylene glycol),[82,83] cyclopropy-lammonium poly(ethylene glycol),[82,83] polyvinyl amine hydroiodide (PVAm HI),[84] etc.). Interestingly, rather than the PEA$^+$ based 2D PVSK (e.g., PEA$_2$PbI$_4$[85]), the PEAI acts as an effective passivation additive for a 3D PVSK.[79,80] Lee et al.[79] reported the use of PEAI for post-treatment of (FAPbI$_3$)$_{0.85}$(MAPbBr$_3$)$_{0.15}$ thin films. Based on their Kelvin probe force microscopy measurement, GBs are passivated after the incorporation of PEA$^+$. The passivation of GBs results in a higher PL intensity and longer carrier lifetimes. Later on, Jiang et al.[80] developed a strategy of using PEAI for FA$_{1-x}$MA$_x$PbI$_3$ surface passivation. The key factor for achieving a high-performance cell is to control the conversion process from PEAI to PEA$_2$PbI$_4$. The PVSK thin film devices with the existence of PEAI rather than PEA$_2$PbI$_4$ achieved a certified PCE of 23.32% (V_{oc} = 1.18 V). Apart from the boosted performance, the long-term stability of the device was significantly improved after the surface passivation. Li et al.[84] achieved compact pinhole-free PVSK by incorporation the additive of polyvinyl amine hydroiodide (PVAm HI). Remarkably, the polymer additive PVAm HI suppressed the defects at the interface and strengthened the interface adhesion of perovskites and ETL/HTL. A champion device with PCE of 16.3% was obtained, and the long-term stability of PSCs was remarkably improved. These unpacked cells yield 92% and 80% of the original efficiency after being exposed under the ambient condition for 50 and 100 days, respectively.

3.3. 2D PVSK

Despite 3D MAPbI$_3$ showing remarkable photoelectric properties and low-temperature processability, the stability of PVSK remains of foremost concern and hinders its commercialization. To address this issue, 2D PVSK been developed as the light absorber material. The chemical formula 2D PVSK is A$_2$B$_{n2}$M$_n$X$_{3n+1}$, wherein A is the organic cations which act as a spacer between the octahedral PVSK planes. The B, M and

X ions are forming the PVSK framework. There are various organic cations have been proposed including n-butylammonium (BA),[86–90] C$_6$H$_5$(CH$_2$)$_2$NH$_3^+$ (PEA$^+$),[91,92] 2,2′-ethylenediamine cations (EDA^{2+}),[93] propane-1,3-diammonium (PDA),[94] HOOC(CH$_2$)$_4$NH$_3^+$ (AVA$^+$),[95] 5-ammoniumvaleric acid (5-AVA)[96] and etc. These 2D PVSK materials have demonstrated superior moisture-resistance in contrast to 3D MAI-based PVSK, because of its more hydrophobic organic cations surface acting as a self-insulated layer at the surface of 2D PVSK.[86,88,97,98] In addition, 2D PVSK exhibits better photothermal stability and lower bulk recombination rate compared with their 3D counterparts.[99,100] However, the theoretical calculation and experimental investigations have demonstrated that the band structure of 2D PVSK was confined in two dimensions with the direction of reciprocal space corresponding to the stacking axis of the layers.[101–103] Consequently, charge transfer along the stacking axis of the layers is effective, but the electrical conductivity across layers was inferior.[104] Therefore, the inefficient carrier transport in the random-oriented 2D PVSK is one of the main factors for its low efficiency. The 2D perovskites with preferred orientation exhibit better electronic transport properties compared with the randomly oriented one.[86,87] To facilities charge transport in 2D PVSK, researchers have tried strategies including 1) Promoting the vertically oriented 2D PVSK, 2) Reducing the distance between octahedral PVSK planes.

The approaches toward developing the 2D PVSK with preferred orientation include a hot-casting method,[86] incorporating additives,[105,106] and doping FA$^+$ cation, or Cs$^+$ cation,[107,108] etc. **Table 1** summarizes the recent work of performance and stability of 2D and 2D/3D hybrid structure PVSK through different strategies. Tsai et al.[86] produced thin films of 2D (BA)$_2$(MA)$_3$Pb$_4$I$_{13}$ with preferred orientation vertical to the substrate by using a hot-casting method. The crystal structure and electronic band structures of (BA)$_2$(MA)$_3$Pb$_4$I$_{13}$ are illustrated in **Figure 3**a,b, respectively. The preferred vertical-aligned orientation of 2D PVSK greatly facilitates charge transport. As a result, the PCE of the 2D (BA)$_2$(MA)$_3$Pb$_4$I$_{13}$ is boosted from the original 4.73%[109] to 12.52%. Figure 3c shows the experimental and simulated J–V curve under standard AM 1.5G illumination for solar cells based on (BA)$_2$(MA)$_3$Pb$_4$I$_{13}$, and the inset picture shows the device structure. Through this approach, Solar cells yielded high PCE with robust performance. The reported 2D PVSK exhibited outstanding stability against light, humidity, and heat stress. Demonstrated in Figure 3d, nonencapsulated devices retain over 70% of its original PCE after 2050 h under constant, standard (AM 1.5G) illumination. And 2D PVSK shows greater tolerance to moisture. The encapsulated device retains over 80% of its original PCE after 2000 h stored in a humidity chamber with relative humidity (RH) of 65%. Thereafter, Zhang et al.[91] reported a vertically orientated 2D (PEA)$_2$(MA)$_{n1}$Pb$_n$I$_{3n+1}$ (n = 3, 4, 5). A PCE of 11.01% was achieved in their work. The humidity stability test shows that the unencapsulated device maintained its 78.5% output after 160 h storage in the air condition with RH of 55 ± 5%. Apart from the inefficient charge transport, the nonradiative V_{oc} loss is another concern for achieving a high performance PVSK solar cell. Fu et al.[105] demonstrated highly efficient 2D (PEA)$_2$(MA)$_4$Pb$_5$I$_{16}$ based solar cells by simultaneously incorporating additives

Table 1. Summary of strategies for improving the performance and stability of multidimensional perovskite photovoltaics.

	Device architecture	Stability		PCE	Ref.
1	Al/PCBM/(BA)$_2$(MA)$_3$Pb$_4$I$_{13}$/PEDOT:PSS/FTO	2050 h, unencapsulated, 1 sun AM 1.5G illumination, 70% of its original PCE, stored in a dry box; 20 h, unencapsulated, 70% of its original PCE, stored in the dark with humidity of 65%; 3000 h, encapsulated, 1 sun AM 1.5G illumination, near 100% of its original PCE, stored in a dry box; 2000 h, encapsulated, over 80% of its original PCE, stored in the dark with humidity of 65%.	2D	12.52%	[88]
2	ITO/PEDOT:PSS/(PEA)$_2$(MA)$_4$Pb$_5$I$_{16}$/PCBM/BCP/Ag	160 h, unencapsulated, 78.5% of its original PCE, storage in air atmosphere with humidity of 55 ± 5%.	2D	11.01%	[91]
3	ITO/PEDOT: PSS/PDAMA$_{n-1}$Pb$_n$I$_{3n+1}$/C$_{60}$/BCP/Ag	1000 h, encapsulated, 90% of its original PCE, stored in dark with humidity of 85%.	2D	13.0%	[94]
4	FTO/SnO$_2$/PC$_{61}$BM/FA$_{0.83}$Cs$_{0.17}$Pb(I$_y$Br$_{1-y}$)$_3$/spiro-OMeTAD/Au	1000 h, unpacked, sustain 80% of its original PCE, stored in air, and close to 3350 h when encapsulated.	2D	16.9%	[89]
5	FTO/SnO$_2$/PC$_{61}$BM/BA$_{0.09}$(FA$_{0.83}$Cs$_{0.17}$)$_{0.91}$Pb(I$_{0.6}$Br$_{0.4}$)$_3$/spiro-OMeTAD/Au	693 h, unpacked, sustain 80% of its original PCE, stored in air, and close to 3880 h when encapsulated.	2D	17.2%	[89]
6	Carbon/ZrO (meso)/MAPbI$_3$ AVA$_2$PbI$_4$/TiO$_2$ (meso)/TiO$_2$ (compact)/FTO	>10 000 h, 1 sun AM 1.5G illumination, ambient atmosphere, 55°C, encapsulated.	2D/3D	12.9%	[95]
7	Au/spiro-OMe TAD/MAPbI$_3$ AVA$_2$PbI$_4$/TiO$_2$ (meso)/TiO$_2$ (compact)/FTO	300 h, 1 sun AM 1.5G illumination, ambient atmosphere, 45 °C, encapsulated.	2D/3D	14.6%	[95]
8	FTO/TiO$_2$/CsPbI$_3$ 0.025EDAPbI$_4$/spiro-MeOTAD/Ag	1 month, unencapsulated, 84.7% of its original PCE, storage in a dark dry box.	2D/3D	11.8%	[93]
9	ITO/compact-SnO$_2$/PEA$_2$PbI$_4$ FACsPbI$_3$/spiro-MeOTAD/Ag (2D PRK: PEA$_2$PbI$_4$ is located at the GBs of 3D PRK: FACsPbI$_3$)	1392 h, unencapsulated, 98% of its original PCE, stored in dark with humidity <30%.	2D/3D	20.64%	[92]
10	FTO/TiO2/C60/MAPbI3 (BA)2(MA)$_{n-1}$Pb$_n$I$_{3n+1}$/spiro-OMeTAD/Au	30 day, unencapsulated, 84% of its original PCE, stored in dark with humidity of 55%.	2D/3D horizontal	16.50%	[90]
11	FTO/SnO$_2$/PC$_{61}$BM/MAPbI$_3$ MA$_3$Bi$_2$I$_9$/spiro-OMeTAD/Au,	1000 h, unencapsulated, 72.34% of its original PCE, stored in ambient air condition with humidity of ≈30%.	2D/3D	18.97%	[112]
12	ITO/TiO$_2$/PCBB-2CN-2C8/MAPbI$_3$/spiro-OMeTAD/Au	500 h, unencapsulated, 60% of its original PCE stored in the dark, ambient atmosphere, RH 45–50%.	3D	16.81%	[113]
13	FTO/TiO$_2$/MAPbI$_3$ 4% PVAm HI/spiro-MeOTAD/Au	100 days, unencapsulated, 80% of the initial PCE value stored in ambient atmosphere with a RH of 30%.	3D	16.3%	[84]

NH$_4$SCN and NH$_4$Cl. Their work showed that doping the additives induced vertically aligned orientation and enhanced the crystallinity of 2D PVSK. The champion devices delivered a PCE as high as 14.1%. The J_{sc} was significantly boosted from 1.7 to 15.8 mA cm^{-2} after doping the additives. And enhanced V_{oc} has been witnessed, which was due to the improved J_{sc} and suppressed nonradiative recombination.

To address the inferior charge transport across layers, reducing the distance between octahedral PVSK planes is another feasible approach.[110,111] Ma et al.[94] tied to reduce the interlayer distance by replacing the large organic cations with shorter spacer ligands PDA cations. Confirmed by the optoelectronic properties measurements, a unique structure restrains the quantum confinement effect leading to a considerable enhancement in charge separation and mobilities. The improved electric properties of their PDA-based 2D PSC yielded a PCE of 13.0%. Furthermore, the stability tests showed that their PDA-based device shows outstanding moisture-tolerance and thermal stability. The encapsulated devices maintain over

90% of PCE after storage in dark conditions with humidity of 85% for 1000 h. The unpackaged PSCs retain their initial PCE at 70 °C for over 100 h.

3.4. 2D/3D Hybrid Structure PVSK

Despite the impressive performance that 2D PVSK solar cells have achieved, further improvement of its PCE is challenging due to its large exciton binding energy, increased bandgap and inefficient charge transport.[109,114,115] One effective strategy to achieve high performance and ultrastable PVSK solar cell is to incorporate vertically aligned 2D PVSK at the GBs the 3D PVSK.[89,93,95] The vertical 2D PVSK acts as a light absorber layer in the cell and self-packaging layer at the 3D PVSK surface. Therefore, 2D/3D hybrid structure PVSK combined enhanced stability of 2D PVSK with excellent photoelectric properties of the 3D ones.[95] Grancini et al.[95] demonstrated outstanding long-term stability PVSK devices by engineering
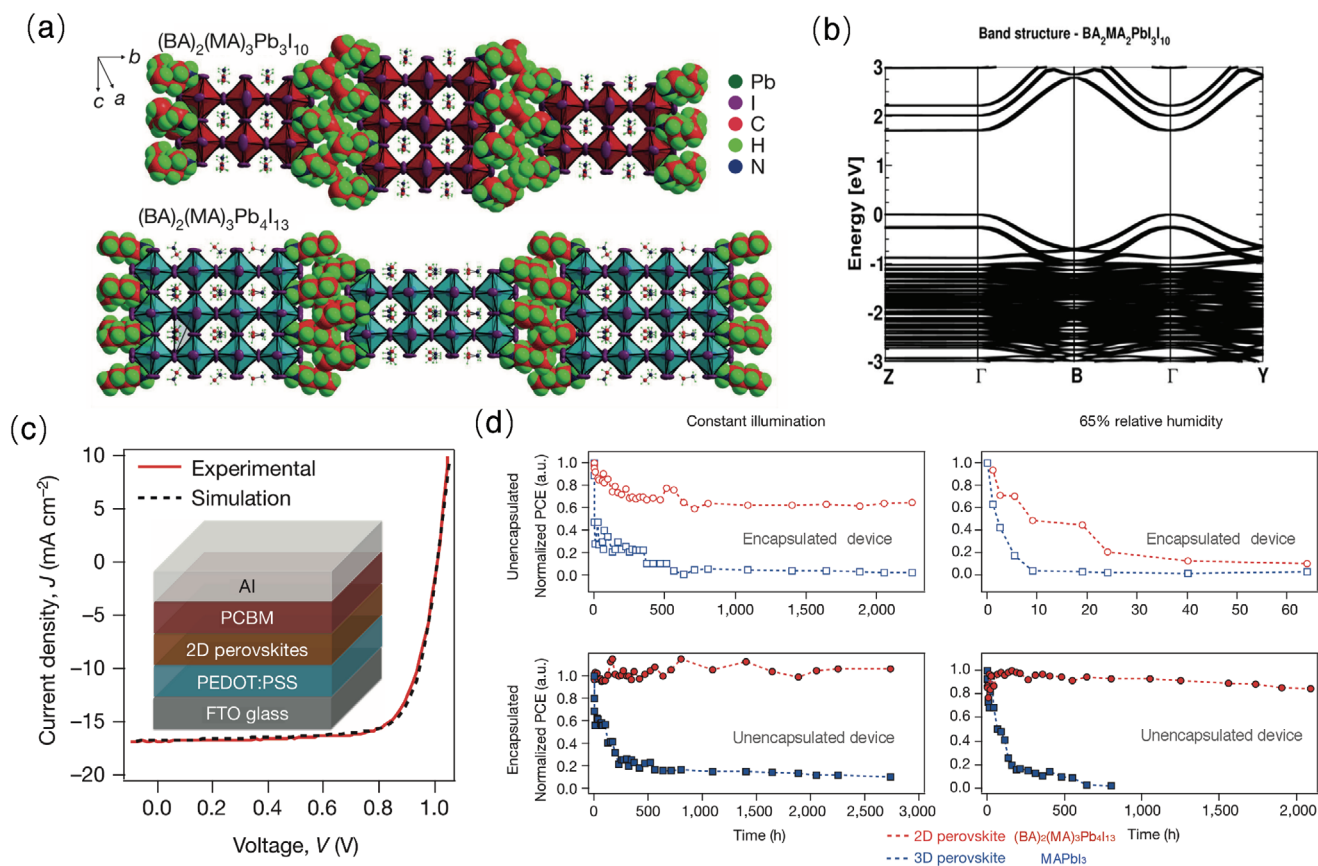
Figure 3. a) The crystal structure of the $(BA)_2(MA)_3Pb_4I_{10}$ and $(BA)_2(MA)_3Pb_4I_{13}$ layered perovskites, the BA spacer layers are depicted as space-fill models to illustrate the termination of the perovskite layers. b) Electronic band structures of and $(BA)_2(MA)_3Pb_4I_{10}$ calculated using DFT with a local-density approximation, including the spin–orbit coupling and a bandgap correction computed using the Heyd–Scuseria–Ernzerhof functional. c) Experimental (red line) and simulated (black dashed line) J–V curves under an AM.1.5G solar simulator for planar devices using 2D $(BA)_2(MA)_3Pb_4I_{13}$ perovskites as the absorbing layer at optimized thickness (230 nm). d) Stability measurements on planar solar cells. Reproduced with permission.[86] Copyright 2016, Springer Nature.

the multidimensional $MAPbI_3/AVA_2PbI_4$. Shown in **Figure 4**a–c, the local density of state (DOS) results reveals that 2D/3D hybrid structure widens the bandgap of 3D PVSK in the interface region. In addition, the 2D PVSK does not hinder the electron injection toward TiO_2. However, it instead suppresses carrier recombination, since the conduction band minimum (CBM) of 2D PVSK locates at the lower energy states of 3D $MAPbI_3$. Shown in Figure 4d, PCEs of 12.9% and 14.6% were realized in carbon-based architecture and standard mesoporous devices, respectively. The corresponding J–V curve can be found in Figure 4e,g,h. Notably, the 2D/3D PVSK exhibits excellent stability against moisture, oxygen, and light. Shown in Figure 4f, the 2D/3D PVSK retained 60% of the initial PCE after 300 h of continuous illumination in the Ar atmosphere. Moreover, shown in Figure 4, the packaged carbon-based device, whose J–V curve were represented in Figure 4g,h, demonstrated remarkable stability of >10 000 h under continuous sun AM 1.5 G illumination at elevated temperature of 55 °C. Similarly, Lee et al.[92] achieved a record efficiency with longevity by forming a 2D/3D hybrid structure. The 2D PEA_2PbI_4 vertically situates between the 3D $FAPbI_3$ grains in order to protect the 3D PVSK against moisture and oxygen and to facilities electron/hole separation and collection. Interestingly, compared

with $FAPbI_3$, the crystallinity of $FAPbI_3$ has been improved after the incorporation of PEA_2PbI_4, which has been verified by a tenfold enhancement in PL lifetime. The enhanced optoelectronic quality of 2D/3D PVSK resulted in a PCE of 20.64% with a peak V_{oc} of 1.130 V. Furthermore, the stability against moisture was greatly enhanced, and the ion migration at GBs was significantly suppressed due to the passivated surface and GBs by incorporation of 2D PEA_2PbI_4. Similarly, Wang and co-workers[87] proposed a strategy of introduction n-butylammonium into $FA_{0.83}Cs_{0.17}Pb(I_yBr_{1-y})_3$. They observed the formation of 2D PVSK at the GBs of 3D PVSK. In addition, the Bi-based 2D PVSK, for instance, $MA_3Bi_2I_9$ and $Cs_3Bi_2I_9$, is a less toxic and more stable potential alternative to Pb-based PVSK.[112] Hu et al.[112] have successfully incorporated vertically aligned $MA_3Bi_2I_9$ platelets with 3D $MAPbI_3$ grains, which combined the merits of the excellent photoelectric property of 3D $MAPbI_3$ and the robust tolerance against moisture and oxygen of 2D $MA_3Bi_2I_9$. Their 2D/3D PVSK cell yielded a PCE of 18.97% with significantly suppressed hysteresis and remarkably enhanced stability.

Another plausible strategy to obtain highly efficient PSCs with longevity is the incorporation of an ultrathin 2D PVSK passivation layer at the interface of 3D PVSK and
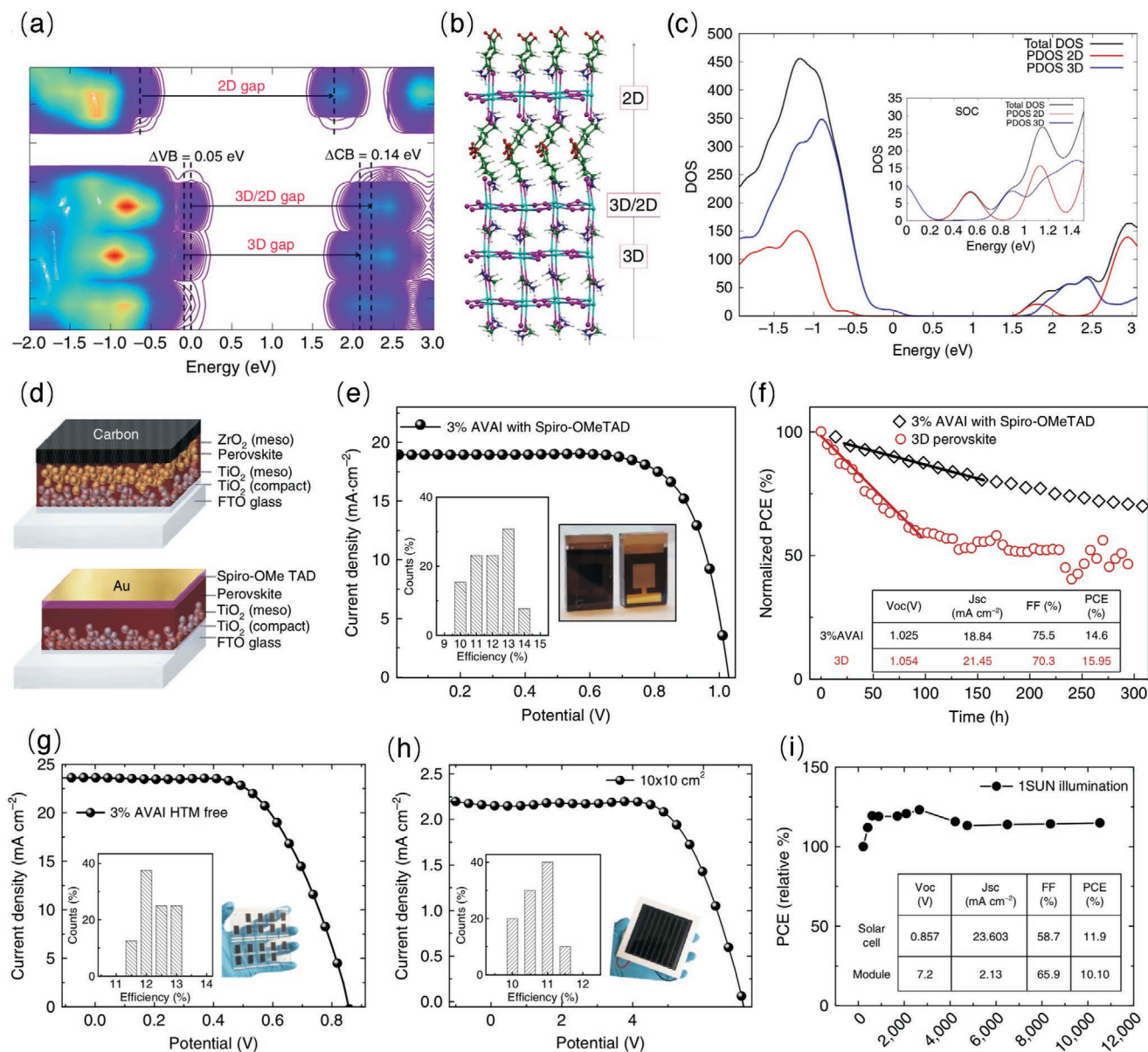
**ADVANCED
SCIENCE NEWS**

www.advancedsciencenews.com

**ADVANCED
MATERIALS
INTERFACES**

www.advmatinterfaces.de

Figure 4. a) The Local density of state (DOS) of the 3D/2D interface. b) Interface structure with the 2D phase contacting the TiO$_2$ surface. c) Partial DOS summed on the 2D and 3D fragments. d) Device cartoon of the Hole transporting Material (HTM)-free solar cell and of the standard HTM-based solar cell. e) J–V curve using the 2D/3D perovskite with 3% HOOC(CH$_2$)$_4$NH$_3$I, AVAI, hereafter, in a standard mesoporous configuration using spiro-OMeTAD/Au (devise statistics and picture of the cell in the inset). f) Stability curve of the spiro-OMeTAD/Au cell comparing standard 3D with the mixed 2D/3D perovskite at maximum power point under AM 1.5G illumination, argon atmosphere and stabilized temperature of 45 °C. The solid line represents the linear fit. In the inset the champion device parameters are listed. g) J–V curve using the 2D/3D perovskite with 3%AVAI in HTM-free solar cell measured under air mass (AM) 1.5G illumination (device statistics and picture in the inset). h) J–V curve using the 2D/3D perovskite with 3%AVAI in a HTM-free 10 × 10 cm^2 module (device statistics and picture in the inset). i) Typical module stability test under 1 sun AM 1.5 G conditions at stabilized temperature of 55 °C at short circuit conditions. Stability measurements were done according to the standard aging conditions. In the inset device parameters of the devices represented in (g,h). Reprinted with permission.[95] Copyright 2017, Nature Research.

HTL. Chen et al.[96] have improved the efficiency and stability of PSCs simultaneously by in situ introduction of passivating layer 2D (5-AVA)$_2$PbI$_4$ at the interface between 3D (FAPbI$_3$)$_{0.88}$(CsPbBr$_3$)$_{0.12}$ and HTL copper(I) thiocyanate (CuSCN). They have witnessed enhanced interfacial charge extraction efficiency and a suppressed carrier recombination after the introduction of (5-AVA)$_2$PbI$_4$ passivation layer, which has been confirmed by enhanced carrier lifetimes, reduced

hysteresis behavior, and raised J_{sc}. As a result, the PCE was boosted from 13.72% to 16.75%. Moreover, superior moisture resistance and photostability were observed in the aging test. The unpackaged device retains 98% of its original PCE after 63 days storage in dark condition with RH of 10%. Soon after, Lin et al.[90] also successfully fabricated 3D MAPbI$_3$/2D (BA)$_2$(MA)$_{n1}$Pb$_n$I$_{3n+1}$ planar hetero-junction through a full vapor strategy. The mixed 3D/2D PVSK exhibited remarkable

ADVANCED
SCIENCE NEWS
www.advancedsciencenews.com

ADVANCED
MATERIALS
INTERFACES
www.advmatinterfaces.de

moisture tolerance and thermal stability. The optimized device demonstrated PCE of 16.50%, and the encapsulated device retained 78.5% of its initial PCE after storage for 30 days with RH of 55% and 72% efficiency after 30 days under 80 °C thermal stress. The superior stability is ascribed to the passivation $(BA)_2(MA)_{n1}Pb_nI_{3n+1}$ layer, which prevents the penetration of moisture and the release of MAI molecules in the $MAPbI_3$.

4. Interface Engineering

Apart from the intrinsic stability issue of PVSK, the moisture or oxygen-induced degradation, as well as the chemical and physical interaction between PVSK with ETL/HTL, are the main contributing factors for the degradation of PSCs. Coating barrier layers on the surface of PVSK has proved to be a practical approach to enhance stability.[116] For instance, Yang et al.[117] successfully fabricated PSCs with great moisture resistance by assembling hydrophobic tertiary and quaternary alkylammonium cations on the top surface of PVSK. Wang et al.[118] in situ inserted a tunneling layer of hydrophobic fluorosilane at the interface between PVSK and ETL to boost the efficiency and stability. The tunneling layer acts as an encapsulation layer to prevent PVSK from decomposition. Moreover, the short current leakage was significantly suppressed after the insertion of the tunneling layer. Recent studies have demonstrated that the interface engineering is far beyond a buffer layer to resist moisture and oxygen. Interface engineering is helpful for achieving highly efficient and robust cells via the control of the interfacial charge extraction in PSCs.[119]

The photogenerated carriers are separated into free charges at the boundary of PVSK and ETL/HTL, and a high-performance cell relies on efficient charge extraction. The interface quality and energy-level alignment are crucial for charge extraction and determine the overall performance of the cell.[120] Therefore, appropriate energy level tailoring at the interface facilitates charge extraction and transfer resulting in enhanced J_{sc}, V_{oc}, and FF. Besides, the engineering for a superior interface quality eliminates the charge loss due to the nonradiative recombination at the interface and gives rise to the charge extraction efficiency consequently. Furthermore, interface engineering is reported as an effective way to eliminate hysteresis behavior[121,122] and improve device stability of PSCs. In this section, we have summarized the recent progress of interface engineering strategy between PVSK and ETL/HTL for high performance and stable PSCs.

4.1. Surface Passivation between PVSK with ETL

Empirically, the uniform coverage of the tunneling layer (e.g., insulating polymer or metal oxide) with a controlled thickness (usually<2 nm) is vital for the performance of cells, thinner or thicker film will undermine the performance of the cell.[123] The reported work shows the 2D materials, including graphene, molybdenum disulfide (MoS_2), etc. are promising candidates for modification of interface properties for PSCs.

With the aim of exploiting the potential of 2D materials for interface engineering, Najafi et al.[124] proposed an approach for the optoelectronic properties tuning of the low-dimensional MoS_2 and reduced graphene oxide (RGO) hybrids. After modification, the hybrid 2D materials possess the electron-blocking property and serve as an active buffer layer in PSCs. The sketch of their device structure and band-energy diagram of the complete device are demonstrated in **Figure 5**a,b. Shown in Figure 5a, the MoS_2/RGO hybrids, which implements hole-transport and electron-blocking properties in a cell, locates between PVSK and HTL in the mesoscopic $MAPbI_3$-based PSCs. The energy band edge positions of their MoS_2 flakes and MoS_2 quantum dots (QDs) were determined from the optical absorption spectroscopy and ultraviolet photoelectron spectroscopy measurements. Owing to quantum confinement effects, the bandgap of MoS_2 is raised from 1.4 eV (MoS_2 flakes) to >3.2 eV (MoS_2 QDs). And CBM is increased from −4.3 eV (MoS_2 flakes) to −2.2 eV (MoS_2 QDs), which is above CBM of $MAPbI_3$ (between −3.7 and −4 eV).[125] Therefore, MoS_2 hybrids possess electron-blocking properties (Figure 5b). As the MoS_2 QDs cannot form a full coverage on the $MAPbI_3$ film surface without any pinhole, Najafi et al. utilized the functionalized RGO to plug in the pinholes of MoS_2 QDs thin film effectively. Consequently, a homogeneous nanometer thick active buffer layer was fabricated. Benefits from better energy level tailoring and superior charge extraction efficiency, the champion device yields a PCE of up to 20.12%. Soon after, Agresti et al.[126] also proposed an interface engineering strategy by using 2D materials including graphene and functionalized MoS_2. The efficiency and stability of PSCs were improved simultaneously after the application of 2D materials. The large-area PSCs were achieved after the introduction of 2D materials, with PCEs of 13.4% and 15.3% over an active area of 108 and 82 cm², respectively. The enhanced performance leads to the highest reported active area-indexed aperture PCE of 1266.5% cm². Besides, the modified devices demonstrated superior thermal stability. The PSCs retained 80% of its initial PCE after 370 h of thermal treatment at 65 °C. Similarly, Zhao et al.[127] modified the interface between ETL nanocrystal SnO_2 with PVSK by incorporation of 2D naphthalene diimide-graphene to augment charge extraction. As a result, highly efficient PSCs with a PCE of 20.2% were obtained with an improved FF of 82%. Agresti et al.[128] exploited the graphene flakes doped with mesoporous TiO_2 (m-TiO_2) and lithium-neutralized graphene oxide flakes as an interlayer to enhance charge injection. The PCE achieved a record of 12.6% with a 50.6 cm² scalable device. Hadadian et al.[129] raised the PCE from 17.3% to 18.7% after introducing nitrogen-doped graphene.

Apart from the better energy-band alignment in a cell, the self-assembled monolayers derived from polarity molecules can work for surface engineering; molecules with polar groups could enhance the contact between ETL and PVSK layer and improve both crystallinity and morphology of PVSK thin films. Yang et al.[130] utilized 3-aminopropyltriethoxysilane assembled monolayer as an interfacial layer between SnO_2 and PVSK. After grain size enlargement and passivated interface importing, their best PCE reached 18% with a negligible hysteresis effect.

Another effective strategy of double-layer ETL for better surface coverage, energetic alignment and higher carrier transport efficiencies was proposed recently. Tavakoli et al.[122] studied the
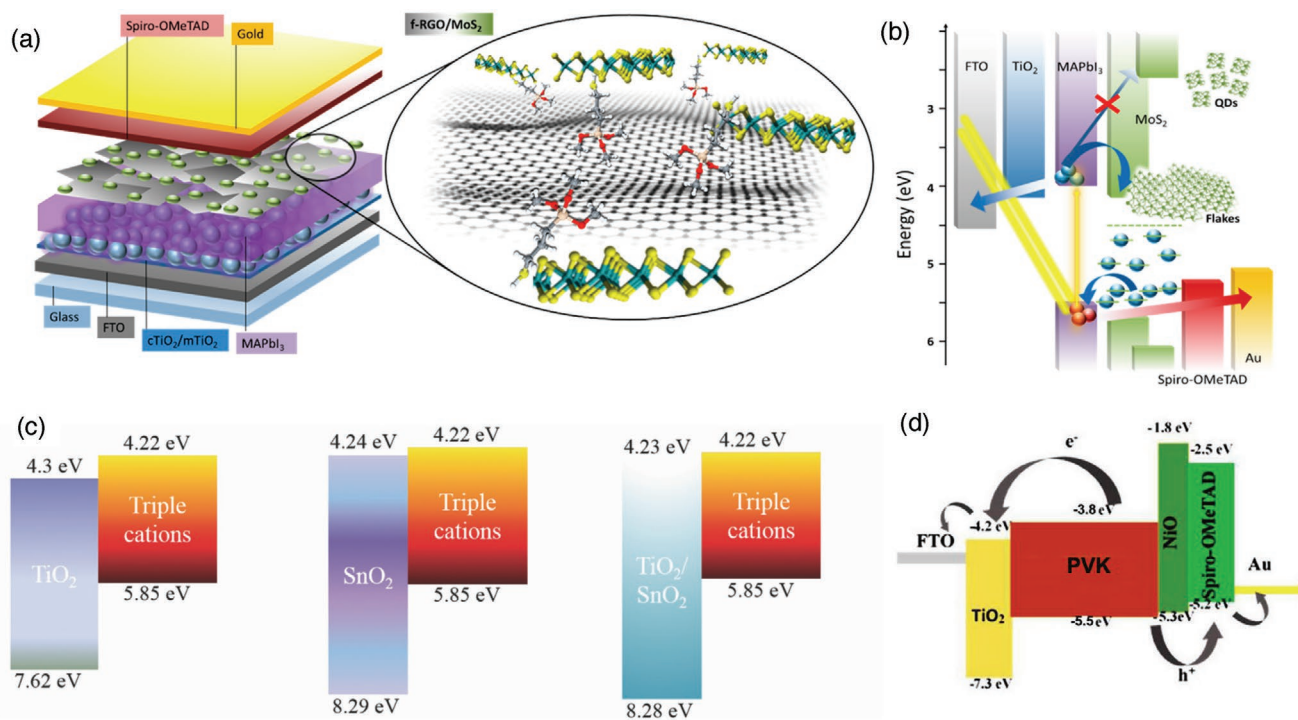
Figure 5. a) Sketch of PSCs exploiting MoS₂ QDs/f-RGO hybrids for interface engineering. b) Band-energy diagram of the complete device in (a). c) Schematics of band alignment for devices based on c-TiO₂, a-SnO₂, and a-SnO₂/c-TiO₂ ETLs. d) Energy level diagram of the planar PSC with a NiO thin film in the interface of PVK/spiro-OMeTAD (the corresponding energy levels are extracted from literature).[157–161] a,b) Reproduced with permission.[124] Copyright 2018, American Chemical Society. c,d) Reproduced with permission.[123] Copyright 2019, Elsevier Ltd.

band alignment engineering on the performance of PSCs. The interface between compact TiO₂ (c-TiO₂) and PVSK is modified by the insertion of a layer of amorphous SnO₂ (a-SnO₂). As demonstrated in Figure 5c,d, the double layer ETL structure of c-TiO₂/a-SnO₂ modified the interface energetics and contributed to efficient charge extraction. As a result, the PCE was effectively improved from 19.33% (c-TiO₂ based device) to 21.4% (c-TiO₂/a-SnO₂ based device). Notably, the optimized device exhibits a maximum V_{oc} of 1.223 V, which is among the record-high values for PSCs with negligible hysteresis. Moreover, the modified devices show better stability, with 91% and 67% of its initial PCE for c-TiO₂/a-SnO₂ based devices and pure c-TiO₂ based devices after 500 h of light illumination, respectively. Thereafter, Liu et al.[131] also witnessed a superior electron extraction capability of c-TiO₂/a-SnO₂ compared the pure c-TiO₂. The superior performance double layer ETL can be ascribed to the improved surface morphology, mitigated current shunting pathways and high mobility of a-SnO₂. Consequently, a cost-effective, stable high-performance all-inorganic CsPbBr₃ based PSCs were achieved. The champion device showed a record-high PCE of 8.79%. The device yields decent efficiency with robustness. The unpackaged devices show excellent stability with no decline in PCE when stored in ambient air condition with RH of 40% at 25 °C for over 1000 h and 60 °C for 720 h. Tan et al.[132] proposed a contact-passivation method by introducing a chlorine-capped TiO₂ colloidal nanocrystal film, which suppresses interfacial nonradiative recombination and improves interface binding of PSCs. The device exhibited a PCE of 21.4% (V_{oc} = 1.189 V, J_{sc} = 22.3 mA cm⁻², FF = 0.806) without obvious hysteresis in J–V sweeps. Ravishankar et al.[133]

deposited m-TiO₂ onto the c-TiO₂ layer. The device based on the m-TiO₂/c-TiO₂ exhibits a PCE of 18.75%, which is higher than the c-TiO₂ (PCE = 16.25%) and the ETL-free devices (PCE = 4.03%). Yan et al.[134] explored a SnO₂/ZnO double-layer ETL in the PSCs for a better carrier extraction and energetic alignment. As a result, their all-inorganic PSCs achieved a PCE of 14.6%. Li and co-workers[135] boosted the PCE of their PSCs from 11.5% to 15.3% by the surface treatment of CsBr on c-TiO₂. Kam et al.[136] tried to replace the solution-processed TiO₂ by exploring the method of sputtering SnO₂ as an ETL.

4.2. Surface Passivation between PVSK with HTL

The passivation of the HTL (hole transport layer) is a practical approach to improve the device longevity and performance further. The most widely used 2,2′,7,7′-tetrakis(*N,N*-di-*p*-methoxyphenylamine)-9,9′-spirobifluorene (spiro-MeOTAD) in PSCs requires the dopants of lithium bistrifluoromethanesulfonimidate (Li-TFSI),[137] which is hygroscopic and aggravates the moisture-induced degradation.[138] In addition, the weak adhesion of mild organic HTL to the PVSK surface can lead to a loss of PCE.[139]

Adoption of the hydrophobic HTL[140–142] or a carbon-based electrode in an HTL-free PSC[143] can effectively improve the device longevity. However, these strategies subsequently sacrifice the efficiency of the solar cell. To address these issues, the alternative inorganic materials serving as HTL or active buffer layers have been explored, for instance, NiO,[123,144] Al₂O₃,[145] copper thiocyanate (CuSCN),[146–148] copper iodide (CuI),[149]

copper oxides (Cu_2O[150] and CuO[151]), etc. Zhang et al.[123] utilized p-type NiO nanocrystals as an active buffer layer. The device structure and energy-band diagram of the device is demonstrated in Figure 5d. Interestingly, they have found the NiO thin films significantly eliminated charge accumulation at the interface of spiro-MeOTAD and PVSK. Whereas, the thickness of NiO films is not critical for the solar cell performance. Because of the optimized interface quality, a champion device with a PCE of 19.89% was achieved. Furthermore, their device demonstrated remarkable long-term stability. Their device retained 94.40% of the original PCE after 400 h storage in ambient condition with RH of 50 ± 5%. Soon after, Pang et al.[144] proposed a novel solution-free process to fabricate the NiO_x thin layer with controlled thickness. The results demonstrate that the NiO_x is a promising HTL in PSCs with excellent energy alignment in a cell, high light transmittance, and outstanding charge-extracting capacity. Koushik et al.[145] introducing an ultrathin layer Al_2O_3 at the interface of the spiro-MeOTAD and PVSK by the atomic layer deposition. The uniform coverage of Al_2O_3 protected the PVSK from moisture and oxygen ingression. The ultrathin thickness of Al_2O_3 makes it possible to achieve a tunnel contact. The optimized device demonstrated remarkable performance with a stabilized PCE of 18%, suppressed hysteresis, and outstanding long-term stability. The unpackaged device retains about 60–70% of initial PCE after 70 days of storage in the ambient condition with humidity of 40–70%.

Several investigations have found that the interfacial defects are charge accumulation centers during the device operation and accelerate the degradation process.[152] To minimize the density of defects at the interface. Abdi-Jalebi et al.[152] proposed a thermal evaporation strategy to incorporate dopant-free tetracene at the interface of spiro-OMeTAD and PVSK. The optimized device exhibited excellent performance with a PCE up to 21.6% and high stability. Their PSCs extended 90% of its original PCE after over 550 h of continuous illumination at AM1.5G. Yang and co-workers[153] also found that the incorporation of the passivation layer contributes to the improvement of solar cell efficiency and stability simultaneously. A highly efficient PSCs (PCE = 20.4%.) with long-term stability was obtained by introducing a layer of poly(methyl methacrylate) (PMMA) at the interface of the PVSK and spiro-OMeTAD in the $MAPbI_3$ PSCs. In addition, Correa-Baena et al.[154] discovered the recombination dynamics is strongly related to Li-TFSI dopant concentration. Zeng et al.[155] exploited the potential of poly(3-hexylthiophene) (P3HT) as a passivating layer in PSCs. Liu et al.[156] introduced $CsPbI_3$ QDs as a tunneling layer between PVSK and HTL. By synergistically controlling the energy level tailoring at the interface, the efficacy of hole transfer has been successfully improved. The PCE has been subsequently raised from 15.17% to 18.56%. Furthermore, the optimized device exhibited better long-term stability and hydro resistance.

5. Outlook

Though PCEs reaching 25.2% have been achieved in PSCs, a practical application still requires further development of high-performance cell with longevity. Notably, the stability is the core issue and must be solved before considering commercialization. The lifetime of perovskites has been significantly engendered from a few minutes to ten thousands of hours by interfacial engineering. But it is still far away from being commercially viable. Future work requires to upgrade the lifetime to ten years or even longer. In addition, it is urgently needed to develop a standard for PVSK stability tests in order to have a better comparison of different strategies. The strategies summarized above encompassing intralayer GBs engineering, as well as the interface optimization between various layers in the cell, provide feasible approaches to advance PSCs toward practical application further.

The 2D/3D PVSK has exhibited the breakthrough point to improve device longevity. The lifetime and performance of the device have been remarkably upgraded through 2D or 2D/3D PVSK structure design, cation engineering, etc. Also, due to its unique physical features, the low-dimensional perovskites offer the possibility for new applications such as flexible and wearable devices, high-performance tandem devices, and semi-transparent cells, etc. In spite of the promising potential, still, a lot of theoretical and experimental efforts need to be exerted to reach the state-of-the-art, such as the uncontrollable distribution of 2D in 3D phases through the solution process,[89,90] the understanding of reaction mechanism 2D/3D PVSK and a feasible strategy for scalability of fabrication. More importantly, there is a complex dilemma to balance the moisture resistance with the electrical conductivity in 2D PVSK. Moreover, the engineering of the perovskites lattice structure and device architecture is an intricate work, and even a small change will impact the overall performance of the device. Nevertheless, the fundamental knowledge of low-dimensional perovskites is still limited. Therefore, in-depth characterization is needed in order to have a better understanding of electrical properties, light coupling properties, trap states, and degradation processes in the 2D and 2D/3D perovskite. Especially, comprehension and control of charge transport will be the critical aspect for the research of low-dimensional perovskites. The insights of these fundamental works could lead to more rational design for the optimal perovskites lattice structure and device architecture with a specific requirement.

Despite that, there are still controversial opinions toward the impact of PVSK GBs on the performance and stability of this device. Undoubtedly, GBs play an instrumental role in shaping the optoelectronic properties and degradation processes. Extensive work has already demonstrated the intralayer GBs engineering is a practical approach for improving device performance and stability. Apart from the low-dimensional PVSK engineering, strategies such as perovskites crystal-size optimization, grain boundary passivation also effectively suppressed the impact of ion migration and defects at GBs. However, massive efforts are still required to have a better understanding of the role of GBs, for example, ion migration, impurities, dangling bonds, charge transfer, and recombination kinetics at GBs. Moreover, the perovskites' crystallization mechanism and the molecular passivation mechanism have not been fully understood. Appropriate additive passivation strategy for high-quality PVSK thin films with high coverage and uniformity will be a solution for stable, high-performance cell and meets the industrial standards.

**ADVANCED
SCIENCE NEWS**

www.advancedsciencenews.com

**ADVANCED
MATERIALS
INTERFACES**

www.advmatinterfaces.de

The interface between PVSK and ETL/HTL is the junction where photogenerated excitons are dissociated into free charges, and the overall performance of solar cells depends on the efficient carrier dissociation and extraction. The PCE of PSCs has been remarkably enhanced through interface optimization for a better interface quality, interfacial band bending, and alignment. Whereas these properties will strongly affect the aging process of perovskites and interaction between PVSK with ETL/HTL layer, it will also change during device operation. Moreover, the extraction efficiency of electrons will be affected by the hole extraction efficiency and vice versa. Therefore, an in-depth understanding of these properties and kinetics at interfaces is required. In particular, it is needed to form a full understanding of the physical and chemical interactions at the interface of PVSK and ETL/HTL and their impact on device characteristics (for instance, the carrier extraction efficiency, recombination kinetics and the degradation process). Furthermore, efforts should be devoted to device architecture design optimization and characterization.

Conflict of Interest

The authors declare no conflict of interest.

[1] National Renewable Energy Laboratory, Best Research Cell Efficiencies Chart, https://www.nrel.gov/pv/cell-efficiency.html.

[2] N. K. Noel, A. Abate, S. D. Stranks, E. S. Parrott, V. M. Burlakov, A. Goriely, H. J. Snaith, *ACS Nano* **2014**, *8*, 9815.

[3] M. M. Tavakoli, K.-H. Tsui, Q. Zhang, J. He, Y. Yao, D. Li, Z. Fan, *ACS Nano* **2015**, *9*, 10287.

[4] W. Tress, N. Marinova, O. Inganäs, M. K. Nazeeruddin, S. M. Zakeeruddin, M. Graetzel, *Adv. Energy Mater.* **2015**, *5*, 1400812.

[5] S.-W. Lee, S. Kim, S. Bae, K. Cho, T. Chung, J.-K. Hwang, I. Song, W. Lee, S. Park, J. Jung, J. Chun, Y. J. Lee, Y. J. Moon, H.-S. Lee, D. Kim, C. B. Mo, Y. Kang, *Org. Electron.* **2018**, *63*, 343.

[6] H. Tan, A. Jain, O. Voznyy, X. Lan, F. P. García de Arquer, J. Z. Fan, R. Quintero-Bermudez, M. Yuan, B. Zhang, Y. Zhao, F. Fan, P. Li, L. N. Quan, Y. Zhao, Z.-H. Lu, Z. Yang, S. Hoogland, E. H. Sargent, *Science* **2017**, *355*, 722.

[7] W. S. Yang, B.-W. Park, E. H. Jung, N. J. Jeon, Y. C. Kim, D. U. Lee, S. S. Shin, J. Seo, E. K. Kim, J. H. Noh, S. I. Seok, *Science* **2017**, *356*, 1376.

[8] E. Jokar, C.-H. Chien, A. Fathi, M. Rameez, Y.-H. Chang, E. W.-G. Diau, *Energy Environ. Sci.* **2018**, *11*, 2353.

[9] L. Gu, D. Zhang, M. Kam, Q. Zhang, S. Poddar, Y. Fu, X. Mo, Z. Fan, *Nanoscale* **2018**, *10*, 15164.

[10] S. R. Raga, M.-C. Jung, M. V. Lee, M. R. Leyden, Y. Kato, Y. Qi, *Chem. Mater.* **2015**, *27*, 1597.

[11] J. A. Christians, P. A. Miranda Herrera, P. V. Kamat, *J. Am. Chem. Soc.* **2015**, *137*, 1530.

[12] Q. Wang, B. Chen, Y. Liu, Y. Deng, Y. Bai, Q. Dong, J. Huang, *Energy Environ. Sci.* **2017**, *10*, 516.

[13] J. S. Yun, J. Seidel, J. Kim, A. M. Soufiani, S. Huang, J. Lau, N. J. Jeon, S. I. Seok, M. A. Green, A. Ho-Baillie, *Adv. Energy Mater.* **2016**, *6*, 1600330.

[14] J. S. Yun, J. Kim, T. Young, R. J. Patterson, D. Kim, J. Seidel, S. Lim, M. A. Green, S. Huang, A. Ho-Baillie, *Adv. Funct. Mater.* **2018**, *28*, 1705363.

[15] Y. Shao, Y. Fang, T. Li, Q. Wang, Q. Dong, Y. Deng, Y. Yuan, H. Wei, M. Wang, A. Gruverman, *Energy Environ. Sci.* **2016**, *9*, 1752.

[16] Y. Yuan, J. Huang, *Acc. Chem. Res.* **2016**, *49*, 286.

[17] G. Mariani, A. C. Scofield, C.-H. Hung, D. L. Huffaker, *Nat. Commun.* **2013**, *4*, 1497.

[18] G. Martin, A. Mitonneau, A. Mircea, *Electron. Lett.* **1977**, *13*, 191.

[19] S. Sze, J. Irvin, *Solid-State Electron.* **1968**, *11*, 599.

[20] W. K. Metzger, S. Grover, D. Lu, E. Colegrove, J. Moseley, C. Perkins, X. Li, R. Mallick, W. Zhang, R. Malik, *Nat. Energy* **2019**, *4*, 837.

[21] I. Visoly-Fisher, S. R. Cohen, A. Gartsman, A. Ruzin, D. Cahen, *Adv. Funct. Mater.* **2006**, *16*, 649.

[22] A. G. Aberle, *Prog. Photovoltaics* **2000**, *8*, 473.

[23] C. P. Muzzillo, *Sol. Energy Mater. Sol. Cells* **2017**, *172*, 18.

[24] J. Nelson, *The Physics of Solar Cells*, Imperial College Press, London **2003**.

[25] J. Kim, S.-H. Lee, J. H. Lee, K.-H. Hong, *J. Phys. Chem. Lett.* **2014**, *5*, 1312.

[26] W.-J. Yin, T. Shi, Y. Yan, *Appl. Phys. Lett.* **2014**, *104*, 063903.

[27] A. Buin, P. Pietsch, J. Xu, O. Voznyy, A. H. Ip, R. Comin, E. H. Sargent, *Nano Lett.* **2014**, *14*, 6281.

[28] W. J. Yin, T. Shi, Y. Yan, *Adv. Mater.* **2014**, *26*, 4653.

[29] W. J. Yin, H. Chen, T. Shi, S. H. Wei, Y. Yan, *Adv. Electron. Mater.* **2015**, *1*, 1500044.

[30] Q. Dong, Y. Fang, Y. Shao, P. Mulligan, J. Qiu, L. Cao, J. Huang, *Science* **2015**, *347*, 967.

[31] D. W. de Quilettes, S. M. Vorpahl, S. D. Stranks, H. Nagaoka, G. E. Eperon, M. E. Ziffer, H. J. Snaith, D. S. Ginger, *Science* **2015**, *348*, 683.

[32] D. Shi, V. Adinolfi, R. Comin, M. Yuan, E. Alarousu, A. Buin, Y. Chen, S. Hoogland, A. Rothenberger, K. Katsiev, *Science* **2015**, *347*, 519.

[33] D. Zhang, L. Gu, Q. Zhang, Y. Lin, D.-H. Lien, M. Kam, S. Poddar, E. C. Garnett, A. Javey, Z. Fan, *Nano Lett.* **2019**, *19*, 2850.

[34] W. Nie, H. Tsai, R. Asadpour, J.-C. Blancon, A. J. Neukirch, G. Gupta, J. J. Crochet, M. Chhowalla, S. Tretiak, M. A. Alam, *Science* **2015**, *347*, 522.

[35] G. Xing, N. Mathews, S. Sun, S. S. Lim, Y. M. Lam, M. Grätzel, S. Mhaisalkar, T. C. Sum, *Science* **2013**, *342*, 344.

[36] R. Long, J. Liu, O. V. Prezhdo, *J. Am. Chem. Soc.* **2016**, *138*, 3884.

[37] H.-S. Duan, H. Zhou, Q. Chen, P. Sun, S. Luo, T.-B. Song, B. Bob, Y. Yang, *Phys. Chem. Chem. Phys.* **2015**, *17*, 112.

[38] C. G. Bischak, E. M. Sanehira, J. T. Precht, J. M. Luther, N. S. Ginsberg, *Nano Lett.* **2015**, *15*, 4799.

[39] A. Waleed, M. M. Tavakoli, L. Gu, S. Hussain, D. Zhang, S. Poddar, Z. Wang, R. Zhang, Z. Fan, *Nano Lett.* **2017**, *17*, 4951.

[40] A. Waleed, M. M. Tavakoli, L. Gu, Z. Wang, D. Zhang, A. Manikandan, Q. Zhang, R. Zhang, Y.-L. Chueh, Z. Fan, *Nano Lett.* **2017**, *17*, 523.

[41] B. Li, M. Li, C. Fei, G. Cao, J. Tian, *J. Mater. Chem. A* **2017**, *5*, 24168.

[42] B. Wang, K. Y. Wong, S. Yang, T. Chen, *J. Mater. Chem. A* **2016**, *4*, 3806.

[43] Z. Xiao, Q. Dong, C. Bi, Y. Shao, Y. Yuan, J. Huang, *Adv. Mater.* **2014**, *26*, 6503.

[44] J. Liu, C. Gao, X. He, Q. Ye, L. Ouyang, D. Zhuang, C. Liao, J. Mei, W. Lau, *ACS Appl. Mater. Interfaces* **2015**, *7*, 24008.

[45] N. Giesbrecht, J. Schlipf, L. Oesinghaus, A. Binek, T. Bein, P. Müller-Buschbaum, P. Docampo, *ACS Energy Lett.* **2016**, *1*, 150.

[46] B. S. Tosun, H. W. Hillhouse, *J. Phys. Chem. Lett.* **2015**, *6*, 2503.

[47] Q. Dong, Y. Yuan, Y. Shao, Y. Fang, Q. Wang, J. Huang, *Energy Environ. Sci.* **2015**, *8*, 2464.

[48] P. W. Liang, C. Y. Liao, C. C. Chueh, F. Zuo, S. T. Williams, X. K. Xin, J. Lin, A. K. Y. Jen, *Adv. Mater.* **2014**, *26*, 3748.

[49] B. Li, D. Binks, G. Cao, J. Tian, *Small* **2019**, *15*, 1903613.

[50] D. Bi, C. Yi, J. Luo, J.-D. Décoppet, F. Zhang, S. M. Zakeeruddin, X. Li, A. Hagfeldt, M. Grätzel, *Nat. Energy* **2016**, *1*, 16142.

[51] A. Cacciuto, S. Auer, D. Frenkel, *Nature* **2004**, *428*, 404.

[52] S. Auer, D. Frenkel, *Nature* **2001**, *413*, 711.

[53] M. M. Tavakoli, S. M. Zakeeruddin, M. Grätzel, Z. Fan, *Adv. Mater.* **2018**, *30*, 1705998.

[54] M. Kam, Y. Zhu, D. Zhang, L. Gu, J. Chen, Z. Fan, *Sol. RRL* **2019**, *3*, 1900050.

[55] M. M. Tavakoli, A. Simchi, X. Mo, Z. Fan, *Mater. Chem. Front.* **2017**, *1*, 1520.

[56] S. Z. Oener, P. Khoram, S. Brittman, S. A. Mann, Q. Zhang, Z. Fan, S. W. Boettcher, E. C. Garnett, *Nano Lett.* **2017**, *17*, 6557.

[57] W. Tress, J. P. Correa Baena, M. Saliba, A. Abate, M. Graetzel, *Adv. Energy Mater.* **2016**, *6*, 1600396.

[58] B. Wu, H. T. Nguyen, Z. Ku, G. Han, D. Giovanni, N. Mathews, H. J. Fan, T. C. Sum, *Adv. Energy Mater.* **2016**, *6*, 1600551.

[59] Y. Shao, Z. Xiao, C. Bi, Y. Yuan, J. Huang, *Nat. Commun.* **2014**, *5*, 1.

[60] J. Xu, A. Buin, A. H. Ip, W. Li, O. Voznyy, R. Comin, M. Yuan, S. Jeon, Z. Ning, J. J. McDowell, *Nat. Commun.* **2015**, *6*, 1.

[61] A. Abate, M. Saliba, D. J. Hollman, S. D. Stranks, K. Wojciechowski, R. Avolio, G. Grancini, A. Petrozza, H. J. Snaith, *Nano Lett.* **2014**, *14*, 3247.

[62] S. D. Stranks, G. E. Eperon, G. Grancini, C. Menelaou, M. J. Alcocer, T. Leijtens, L. M. Herz, A. Petrozza, H. J. Snaith, *Science* **2013**, *342*, 341.

[63] C. Wehrenfennig, M. Liu, H. J. Snaith, M. B. Johnston, L. M. Herz, *Energy Environ. Sci.* **2014**, *7*, 2269.

[64] Y. Tidhar, E. Edri, H. Weissman, D. Zohar, G. Hodes, D. Cahen, B. Rybtchinski, S. Kirmayer, *J. Am. Chem. Soc.* **2014**, *136*, 13249.

[65] S. T. Williams, F. Zuo, C.-C. Chueh, C.-Y. Liao, P.-W. Liang, A. K.-Y. Jen, *ACS Nano* **2014**, *8*, 10640.

[66] L. Zhang, F. Yu, L. Chen, J. Li, *Appl. Surf. Sci.* **2018**, *443*, 176.

[67] S. Yang, S. Chen, E. Mosconi, Y. Fang, X. Xiao, C. Wang, Y. Zhou, Z. Yu, J. Zhao, Y. Gao, *Science* **2019**, *365*, 473.

[68] L. Liu, W.-H. Fang, R. Long, O. V. Prezhdo, *J. Phys. Chem. Lett.* **2018**, *9*, 1164.

[69] X. Zheng, B. Chen, J. Dai, Y. Fang, Y. Bai, Y. Lin, H. Wei, X. C. Zeng, J. Huang, *Nat. Energy* **2017**, *2*, 17102.

[70] X. Li, M. I. Dar, C. Yi, J. Luo, M. Tschumi, S. M. Zakeeruddin, M. K. Nazeeruddin, H. Han, M. Grätzel, *Nat. Chem.* **2015**, *7*, 703.

[71] A. J. Lehner, H. Wang, D. H. Fabini, C. D. Liman, C.-A. Hébert, E. E. Perry, M. Wang, G. C. Bazan, M. L. Chabinyc, R. Seshadri, *Appl. Phys. Lett.* **2015**, *107*, 131109.

[72] S. Ye, H. Rao, Z. Zhao, L. Zhang, H. Bao, W. Sun, Y. Li, F. Gu, J. Wang, Z. Liu, *J. Am. Chem. Soc.* **2017**, *139*, 7504.

[73] J. Xu, A. Buin, A. H. Ip, W. Li, O. Voznyy, R. Comin, M. Yuan, S. Jeon, Z. Ning, J. J. McDowell, *Nat. Commun.* **2015**, *6*, 7081.

[74] D.-Y. Son, J.-W. Lee, Y. J. Choi, I.-H. Jang, S. Lee, P. J. Yoo, H. Shin, N. Ahn, M. Choi, D. Kim, N.-G. Park, *Nat. Energy* **2016**, *1*, 16081.

[75] J. Cao, X. Jing, J. Yan, C. Hu, R. Chen, J. Yin, J. Li, N. Zheng, *J. Am. Chem. Soc.* **2016**, *138*, 9919.

[76] A. Buin, R. Comin, J. Xu, A. H. Ip, E. H. Sargent, *Chem. Mater.* **2015**, *27*, 4405.

[77] W. S. Yang, B.-W. Park, E. H. Jung, N. J. Jeon, Y. C. Kim, D. U. Lee, S. S. Shin, J. Seo, E. K. Kim, J. H. Noh, *Science* **2017**, *356*, 1376.

[78] J. Li, X. Guan, C. Wang, H. C. Cheng, R. Ai, K. Yao, P. Chen, Z. Zhang, X. Duan, X. J. S. Duan, *Small* **2017**, *13*, 1701034.

[79] D. S. Lee, J. S. Yun, J. Kim, A. M. Soufiani, S. Chen, Y. Cho, X. Deng, J. Seidel, S. Lim, S. Huang, *ACS Energy Lett.* **2018**, *3*, 647.

[80] Q. Jiang, Y. Zhao, X. Zhang, X. Yang, Y. Chen, Z. Chu, Q. Ye, X. Li, Z. Yin, J. You, *Nat. Photonics* **2019**, *13*, 460.

[81] Y. Hu, J. Schlipf, M. Wussler, M. L. Petrus, W. Jaegermann, T. Bein, P. Müller-Buschbaum, P. Docampo, *ACS Nano* **2016**, *10*, 5999.

[82] C.-Y. Chang, C.-Y. Chu, Y.-C. Huang, C.-W. Huang, S.-Y. Chang, C.-A. Chen, C.-Y. Chao, W.-F. Su, *ACS Appl. Mater. Interfaces* **2015**, *7*, 4955.

[83] Y. Zhao, J. Wei, H. Li, Y. Yan, W. Zhou, D. Yu, Q. Zhao, *Nat. Commun.* **2016**, *7*, 10228.

[84] H. Li, C. Liang, Y. Liu, Y. Zhang, J. Tong, W. Zuo, S. Xu, G. Shao, S. Cao, *ACS Appl. Mater. Interfaces* **2017**, *9*, 6064.

[85] P. Chen, Y. Bai, S. Wang, M. Lyu, J. H. Yun, L. Wang, *Adv. Funct. Mater.* **2018**, *28*, 1706923.

[86] H. Tsai, W. Nie, J.-C. Blancon, C. C. Stoumpos, R. Asadpour, B. Harutyunyan, A. J. Neukirch, R. Verduzco, J. J. Crochet, S. J. N. Tretiak, *Nature* **2016**, *536*, 312.

[87] Z. Xiao, W. Meng, J. Wang, D. B. Mitzi, Y. Yan, *Mater. Horiz.* **2017**, *4*, 206.

[88] H. Tsai, W. Nie, J.-C. Blancon, C. C. Stoumpos, R. Asadpour, B. Harutyunyan, A. J. Neukirch, R. Verduzco, J. J. Crochet, S. Tretiak, L. Pedesseau, J. Even, M. A. Alam, G. Gupta, J. Lou, P. M. Ajayan, M. J. Bedzyk, M. G. Kanatzidis, A. D. Mohite, *Nature* **2016**, *536*, 312.

[89] Z. Wang, Q. Lin, F. P. Chmiel, N. Sakai, L. M. Herz, H. J. Snaith, *Nat. Energy* **2017**, *2*, 17135.

[90] D. Lin, T. Zhang, J. Wang, M. Long, F. Xie, J. Chen, B. Wu, T. Shi, K. Yan, W. Xie, P. Liu, J. Xu, *Nano Energy* **2019**, *59*, 619.

[91] X. Zhang, G. Wu, W. Fu, M. Qin, W. Yang, J. Yan, Z. Zhang, X. Lu, H. Chen, *Adv. Energy Mater.* **2018**, *8*, 1702498.

[92] J.-W. Lee, Z. Dai, T.-H. Han, C. Choi, S.-Y. Chang, S.-J. Lee, N. De Marco, H. Zhao, P. Sun, Y. Huang, Y. Yang, *Nat. Commun.* **2018**, *9*, 3021.

[93] T. Zhang, M. I. Dar, G. Li, F. Xu, N. Guo, M. Grätzel, Y. Zhao, *Sci. Adv.* **2017**, *3*, e1700841.

[94] C. Ma, D. Shen, T.-W. Ng, M.-F. Lo, C.-S. Lee, *Adv. Mater.* **2018**, *30*, 1800710.

[95] G. Grancini, C. Roldán-Carmona, I. Zimmermann, E. Mosconi, X. Lee, D. Martineau, S. Narbey, F. Oswald, F. De Angelis, M. Graetzel, *Nat. Commun.* **2017**, *8*, 15684.

[96] J. Chen, J.-Y. Seo, N.-G. Park, *Adv. Energy Mater.* **2018**, *8*, 1702714.

[97] L. N. Quan, M. Yuan, R. Comin, O. Voznyy, E. M. Beauregard, S. Hoogland, A. Buin, A. R. Kirmani, K. Zhao, A. Amassian, D. H. Kim, E. H. Sargent, *J. Am. Chem. Soc.* **2016**, *138*, 2649.

[98] S. Ahmad, P. K. Kanaujia, H. J. Beeson, A. Abate, F. Deschler, D. Credgington, U. Steiner, G. V. Prakash, J. J. Baumberg, *ACS Appl. Mater. Interfaces* **2015**, *7*, 25227.

[99] Y. Bekenstein, B. A. Koscher, S. W. Eaton, P. Yang, A. Paul Alivisatos, *J. Am. Chem. Soc.* **2015**, *137*, 16008.

[100] Q. A. Akkerman, S. G. Motti, A. R. Srimath Kandada, E. Mosconi, V. D'Innocenzo, G. Bertoni, S. Marras, B. A. Kamino, L. Miranda, F. De Angelis, A. Petrozza, *J. Am. Chem. Soc.* **2016**, *138*, 1010.

[101] L. Mao, C. C. Stoumpos, M. G. Kanatzidis, *J. Am. Chem. Soc.* **2018**, *141*, 1171.

[102] L. Pedesseau, J.-M. Jancu, A. Rolland, E. Deleporte, C. Katan, J. Even, *Opt. Quantum Electron.* **2014**, *46*, 1225.

**ADVANCED
SCIENCE NEWS**

www.advancedsciencenews.com

**ADVANCED
MATERIALS
INTERFACES**

www.advmatinterfaces.de

[103] L. Dou, A. B. Wong, Y. Yu, M. Lai, N. Kornienko, S. W. Eaton, A. Fu, C. G. Bischak, J. Ma, T. Ding, *Science* **2015**, *349*, 1518.

[104] Y. Zhu, Q. Zhang, M. Kam, S. Poddar, L. Gu, S. Liang, P. Qi, F. Miao, Z. Fan, *InfoMat* **2019**.

[105] W. Fu, J. Wang, L. Zuo, K. Gao, F. Liu, D. S. Ginger, A. K.-Y. Jen, *ACS Energy Lett.* **2018**, *3*, 2086.

[106] X. Zhang, G. Wu, S. Yang, W. Fu, Z. Zhang, C. Chen, W. Liu, J. Yan, W. Yang, H. Chen, *Small* **2017**, *13*, 1700611.

[107] L. Iagher, L. Etgar, *ACS Energy Lett.* **2018**, *3*, 366.

[108] N. Zhou, Y. Shen, L. Li, S. Tan, N. Liu, G. Zheng, Q. Chen, H. Zhou, *J. Am. Chem. Soc.* **2018**, *140*, 459.

[109] I. C. Smith, E. T. Hoke, D. Solis-Ibarra, M. D. McGehee, H. I. Karunadasa, *Angew. Chem., Int. Ed.* **2014**, *53*, 11232.

[110] C. Ma, D. Shen, T. W. Ng, M. F. Lo, C. S. Lee, *Adv. Mater.* **2018**, *30*, 1800710.

[111] A. H. Proppe, R. Quintero-Bermudez, H. Tan, O. Voznyy, S. O. Kelley, E. H. Sargent, *J. Am. Chem. Soc.* **2018**, *140*, 2890.

[112] Y. Hu, T. Qiu, F. Bai, W. Ruan, S. Zhang, *Adv. Energy Mater.* **2018**, *8*, 1703620.

[113] Y. Li, Y. Zhao, Q. Chen, Y. Yang, Y. Liu, Z. Hong, Z. Liu, Y.-T. Hsieh, L. Meng, Y. Li, Y. Yang, *J. Am. Chem. Soc.* **2015**, *137*, 15540.

[114] R. L. Milot, R. J. Sutton, G. E. Eperon, A. A. Haghighirad, J. Martinez Hardigree, L. Miranda, H. J. Snaith, M. B. Johnston, L. M. Herz, *Nano Lett.* **2016**, *16*, 7001.

[115] D. H. Cao, C. C. Stoumpos, O. K. Farha, J. T. Hupp, M. G. Kanatzidis, *J. Am. Chem. Soc.* **2015**, *137*, 7843.

[116] C. Liu, W. Ding, X. Zhou, J. Gao, C. Cheng, X. Zhao, B. Xu, *J. Phys. Chem. C* **2017**, *121*, 6546.

[117] S. Yang, Y. Wang, P. Liu, Y.-B. Cheng, H. J. Zhao, H. G. Yang, *Nat. Energy* **2016**, *1*, 15016.

[118] Q. Wang, Q. Dong, T. Li, A. Gruverman, J. Huang, *Adv. Mater.* **2016**, *28*, 6734.

[119] O. Malinkiewicz, A. Yella, Y. H. Lee, G. M. Espallargas, M. Graetzel, M. K. Nazeeruddin, H. J. Bolink, *Nat. Photonics* **2014**, *8*, 128.

[120] Q. Zhang, M. M. Tavakoli, L. Gu, D. Zhang, L. Tang, Y. Gao, J. Guo, Y. Lin, S.-F. Leung, S. Poddar, *Nat. Commun.* **2019**, *10*, 1.

[121] M. Pantaler, K. T. Cho, V. I. Queloz, I. G. García Benito, C. Fettkenhauer, I. Anusca, M. K. Nazeeruddin, D. C. Lupascu, G. Grancini, *ACS Energy Lett.* **2018**, *3*, 1781.

[122] M. M. Tavakoli, P. Yadav, R. Tavakoli, J. Kong, *Adv. Energy Mater.* **2018**, *8*, 1800794.

[123] W. Zhang, X. Zhang, T. Wu, W. Sun, J. Wu, Z. Lan, *Electrochim. Acta* **2019**, *293*, 211.

[124] L. Najafi, B. Taheri, B. Martín-García, S. Bellani, D. Di Girolamo, A. Agresti, R. Oropesa-Nuñez, S. Pescetelli, L. Vesce, E. Calabrò, M. Prato, A. E. Del Rio Castillo, A. Di Carlo, F. Bonaccorso, *ACS Nano* **2018**, *12*, 10736.

[125] S. Olthof, *APL Mater.* **2016**, *4*, 091502.

[126] A. Agresti, S. Pescetelli, A. L. Palma, B. Martín-García, L. Najafi, S. Bellani, I. Moreels, M. Prato, F. Bonaccorso, A. Di Carlo, *ACS Energy Lett.* **2019**, *4*, 1862.

[127] X. Zhao, L. Tao, H. Li, W. Huang, P. Sun, J. Liu, S. Liu, Q. Sun, Z. Cui, L. Sun, Y. Shen, Y. Yang, M. Wang, *Nano Lett.* **2018**, *18*, 2442.

[128] A. Agresti, S. Pescetelli, A. L. Palma, A. E. Del Rio Castillo, D. Konios, G. Kakavelakis, L. Razza, L. Cinà, E. Kymakis, F. Bonaccorso, *ACS Energy Lett.* **2017**, *2*, 279.

[129] M. Hadadian, J. P. Correa-Baena, E. K. Goharshadi, A. Ummadisingu, J. Y. Seo, J. Luo, S. Gholipour, S. M. Zakeeruddin, M. Saliba, A. Abate, *Adv. Mater.* **2016**, *28*, 8681.

[130] G. Yang, C. Wang, H. Lei, X. Zheng, P. Qin, L. Xiong, X. Zhao, Y. Yan, G. Fang, *J. Mater. Chem. A* **2017**, *5*, 1658.

[131] X. Liu, X. Tan, Z. Liu, H. Ye, B. Sun, T. Shi, Z. Tang, G. Liao, *Nano Energy* **2019**, *56*, 184.

[132] H. Tan, A. Jain, O. Voznyy, X. Lan, F. P. G. De Arquer, J. Z. Fan, R. Quintero-Bermudez, M. Yuan, B. Zhang, Y. Zhao, *Science* **2017**, *355*, 722.

[133] S. Ravishankar, S. Gharibzadeh, C. Roldán-Carmona, G. Grancini, Y. Lee, M. Ralaiarisoa, A. M. Asiri, N. Koch, J. Bisquert, M. K. Nazeeruddin, *Joule* **2018**, *2*, 788.

[134] L. Yan, Q. Xue, M. Liu, Z. Zhu, J. Tian, Z. Li, Z. Chen, Z. Chen, H. Yan, H. L. Yip, *Adv. Mater.* **2018**, *30*, 1802509.

[135] W.-B. Zhang, L.-J. Xiang, H.-B. Li, *J. Mater. Chem. A* **2016**, *4*, 19086.

[136] M. Kam, Q. Zhang, D. Zhang, Z. Fan, *Sci. Rep.* **2019**, *9*, 1.

[137] W. H. Nguyen, C. D. Bailie, E. L. Unger, M. D. McGehee, *J. Am. Chem. Soc.* **2014**, *136*, 10996.

[138] J. Liu, Y. Wu, C. Qin, X. Yang, T. Yasuda, A. Islam, K. Zhang, W. Peng, W. Chen, L. Han, *Energy Environ. Sci.* **2014**, *7*, 2963.

[139] Z. Hawash, L. K. Ono, Y. Qi, *Adv. Mater. Interfaces* **2018**, *5*, 1700623.

[140] L. Zheng, Y.-H. Chung, Y. Ma, L. Zhang, L. Xiao, Z. Chen, S. Wang, B. Qu, Q. Gong, *Chem. Commun.* **2014**, *50*, 11196.

[141] T. Leijtens, T. Giovenzana, S. N. Habisreutinger, J. S. Tinkham, N. K. Noel, B. A. Kamino, G. Sadoughi, A. Sellinger, H. J. Snaith, *ACS Appl. Mater. Interfaces* **2016**, *8*, 5981.

[142] Y. S. Kwon, J. Lim, H.-J. Yun, Y.-H. Kim, T. Park, *Energy Environ. Sci.* **2014**, *7*, 1454.

[143] A. Mei, X. Li, L. Liu, Z. Ku, T. Liu, Y. Rong, M. Xu, M. Hu, J. Chen, Y. Yang, *Science* **2014**, *345*, 295.

[144] S. Pang, C. Zhang, H. Dong, D. Chen, W. Zhu, H. Xi, J. Chang, Z. Lin, J. Zhang, Y. Hao, *ACS Appl. Energy Mater.* **2019**, *2*, 4700.

[145] D. Koushik, W. J. Verhees, Y. Kuang, S. Veenstra, D. Zhang, M. A. Verheijen, M. Creatore, R. E. Schropp, *Energy Environ. Sci.* **2017**, *10*, 91.

[146] N. Arora, M. I. Dar, A. Hinderhofer, N. Pellet, F. Schreiber, S. M. Zakeeruddin, M. Grätzel, *Science* **2017**, *358*, 768.

[147] M. Jung, Y. C. Kim, N. J. Jeon, W. S. Yang, J. Seo, J. H. Noh, S. Il Seok, *ChemSusChem* **2016**, *9*, 2592.

[148] K. Zhao, R. Munir, B. Yan, Y. Yang, T. Kim, A. Amassian, *J. Mater. Chem. A* **2015**, *3*, 20554.

[149] S. Uthayaraj, D. Karunarathne, G. Kumara, T. Murugathas, S. Rasalingam, R. Rajapakse, P. Ravirajan, D. Velauthapillai, *Materials* **2019**, *12*, 2037.

[150] L. Lin, L. Jiang, P. Li, B. Fan, Y. Qiu, *J. Phys. Chem. Solids* **2019**, *124*, 205.

[151] Q. Sun, X. Shi, X. Wang, Y. Zhai, L. Gao, Z. Li, Y. Hao, Y. Wu, *Org. Electron.* **2019**, *75*, 105428.

[152] M. Abdi-Jalebi, M. I. Dar, S. P. Senanayak, A. Sadhanala, Z. Andaji-Garmaroudi, L. M. Pazos-Outón, J. M. Richter, A. J. Pearson, H. Sirringhaus, M. Grätzel, *Sci. Adv.* **2019**, *5*, eaav2012.

[153] J. Yao, Z. Zheng, G. Yang, *ACS Appl. Mater. Interfaces* **2018**, *10*, 38166.

[154] J.-P. Correa-Baena, W. Tress, K. Domanski, E. H. Anaraki, S.-H. Turren-Cruz, B. Roose, P. P. Boix, M. Grätzel, M. Saliba, A. Abate, *Energy Environ. Sci.* **2017**, *10*, 1207.

[155] Q. Zeng, X. Zhang, X. Feng, S. Lu, Z. Chen, X. Yong, S. A. Redfern, H. Wei, H. Wang, H. Shen, *Adv. Mater.* **2018**, *30*, 1705393.

[156] C. Liu, M. Hu, X. Zhou, J. Wu, L. Zhang, W. Kong, X. Li, X. Zhao, S. Dai, B. Xu, C. Cheng, *NPG Asia Mater.* **2018**, *10*, 552.

[157] J. Ma, G. Yang, M. Qin, X. Zheng, H. Lei, C. Chen, Z. Chen, Y. Guo, H. Han, X. Zhao, *Adv. Sci.* **2017**, *4*, 1700031.

[158] Y. Bai, X. Meng, S. Yang, *Adv. Energy Mater.* **2018**, *8*, 1701883.

[159] X. Wen, J. Wu, M. Ye, D. Gao, C. Lin, *Chem. Commun.* **2016**, *52*, 11355.

[160] M. M. Byranvand, T. Kim, S. Song, G. Kang, S. U. Ryu, T. Park, *Adv. Energy Mater.* **2018**, *8*, 1702235.

[161] M. Deepa, M. Salado, L. Calio, S. Kazim, S. Shivaprasad, S. Ahmad, *Phys. Chem. Chem. Phys.* **2017**, *19*, 4069.